Supplementary Information

Multi-fold increase in rainforests tipping risk beyond 1.5-2^{o}C warming

Chandrakant Singh[1,2,3,*], Ruud van der Ent[4], Ingo Fetzer[1,2,5], Lan Wang-Erlandsson[1,2,5]

[1]Stockholm Resilience Centre, Stockholm University, Stockholm, Sweden
[2]Bolin Centre for Climate Research, Stockholm University, Stockholm, Sweden
[3]Department of Space, Earth and Environment, Chalmers University of Technology, Gothenburg, Sweden
[4]Department of Water Management, Faculty of Civil Engineering and Geosciences, Delft University of Technology, Delft, The Netherlands
[5]Potsdam Institute for Climate Impact Research, Potsdam, Germany

*Corresponding author; E-mail: chandrakant.singh@su.se

Content

Supplementary Description

Rainforest tipping under future climate change. Forest and savanna exist as alternative stable states (i.e., equilibrium) (Hirota et al., 2011). Here, the stabilising feedbacks acting on the ecosystem keeps them stable, i.e., the ecosystem would not show a change to its structure until the perturbation on the ecosystem pushes it beyond the tipping point, after which the ecosystem stabilises as an alternative stable state (e.g., a forest pushed beyond the tipping point will stabilise as savanna). 'Tipping' refers to the significant reorganisation of the ecosystem structure, and are considered abrupt and difficult to revert due to the influence of amplifying and stabilising feedbacks (Scheffer et al., 2009). Since ESMs can't simulate these tipping points, we have depended on empirical evidence to forcefully simulate rainforest tipping (Supplementary Table 2). Previous studies have projected local-scale rainforest tipping under future climate change based on assumptions about the equilibrium states (Boulton et al., 2013; Staal et al., 2020). Where some have used precipitation (i.e., empirically constructed stability landscape derived from precipitation and tree cover data) (Boulton et al., 2013; Staal et al., 2018; Zemp et al., 2017), others have hardcoded thresholds in model-derived vegetation state (including structure, distribution, or carbon stocks) (Cox et al., 2004; Higgins and Scheiter, 2012; Jones et al., 2009; Parry et al., 2022; Salazar et al., 2007) to simulate tipping (Supplementary Table 2). However, studies projecting rainforest tipping using precipitation acknowledge that the magnitude and duration of water-deficit experienced by the vegetation also affect them at the local scale, which they were not able to operationalise (Staal et al., 2020; Zemp et al., 2017). In contrast, model-simulated vegetation states are not appropriate for projecting tipping due to their strong correlation with temperature and precipitation, and uncertainty due to the lag between forest's response to hydroclimatic perturbation (Boulton et al., 2013; Jones et al., 2009). Therefore, in this study, we use mass-balance derived root zone storage capacity (S_r) to project forest-savanna transition risk under future climate change. S_r not only accounts for the magnitude and duration of water-deficit (Singh et al., 2020), but is also a better metric to assess forest resilience than precipitation (Singh et al., 2022). Furthermore, compared to other statistical metrics (Boulton et al., 2022; Carpenter and Brock, 2006; Dakos et al., 2008; Rocha, 2022), S_r provides an early indication of forest-savanna transition and a more comprehensive understanding of ecosystem dynamics under water-limiting conditions (Singh et al., 2020, 2022).

Supplementary Methods

Calculating root zone storage capacity (S_r). We adopted the root zone storage capacity (S_r) calculation method from Singh et al., (2020). Here, we first calculate the daily water deficit ($D(t)$) using daily estimates of precipitation ($P(t)$) and evaporation ($E(t)$):

$$D(t) = E(t) - P(t) \tag{1}$$

Where *t* denotes the day count since the start of the simulation. The simulation for each grid cell starts in the month with the highest mean monthly precipitation (2001-2012) and runs for a whole year.

Since the 6th Coupled Model Intercomparison Project (CMIP6; for the CMIP6-historical and -SSP estimates, the timeframe considered are 2000-2014 and 2086-2100, respectively) doesn't have daily estimates of evaporation and precipitation for all Earth System Models (ESMs), we directly use:

$$D(t) = E(t_{monthly}) - P(t_{monthly}) \tag{2}$$

Where $t_{monthly}$ denotes the month count since the start of the simulation. The rest of the steps below remain the same for both empirical and model-estimated datasets.

Next, we calculate the accumulated deficit $D_a(t+1)$ at each one-day (one-month for ESMs) timestep for one year such that it is either equal to or more than zero. However, this value is never less than zero since we are calculating a running estimate of root zone storage reservoir size. Furthermore, we assume the excess precipitation to run off as streamflow or groundwater recharge using:

$$D_a(t+1) = \max\{0, D_a(t) + D(t+1)\} \tag{3}$$

This analysis assumes that vegetation adapts and responds to the most critical dry periods it has experienced over the year (Wang-Erlandsson et al., 2016), therefore we compute the largest accumulated deficit per year ($D_{a,y}$) by:

$$D_{a,y} = \max\{D_a(t+1)\} \quad t = 1 : n-1 \tag{4}$$

Where *n* equals the number of days (number of months for CMIP6 datasets) in year *y*. Since this simulation is run for a whole year using precipitation and evaporation estimates, this mass-balance methodology does consider actual seasonal dynamics of precipitation (incoming moisture flux) and evaporation (outgoing moisture fluxes, including evaporation from soil moisture, interception, transpiration and open water; see methods) at temporal timescales.

Although different terrestrial ecosystems (e.g., forest, savanna and grasslands) adapt to different drought return periods (Wang-Erlandsson et al., 2016; de Boer-Euser et al., 2016; Gao et al., 2014). For this study, we use a uniform 20-year drought return period to avoid any artificially introduced transitions between different ecosystems. This we analyse using on the Gumbel extreme value distribution (Gumbel, 1958) and apply it to normalise all $D_{a,y}$. The Gumbel distribution ($F(x)$) is given by:

$$F(x) = \exp\left[-\exp\left[-\frac{(x-\mu)}{\alpha}\right]\right] \tag{5}$$

Where μ and α are the location and scale parameters, respectively. We calculate this using the python package 'skextremes'(skextremes Documentation):

$$S_r = \overline{D_{a,y}} + K \times \sigma_{n-1} \tag{6}$$

where K is the frequency factor given by:

$$K = \frac{y_t - y_n}{S_n} \tag{7}$$

And y_t is the reduced variate given by:

$$y_t = -\left[\ln\left[\ln\left(\frac{T}{T-1}\right)\right]\right] \tag{8}$$

Where T is the drought return period (i.e., 20 years used in this study), $\overline{D_{a,y}}$ is the mean annual accumulated deficit for the years 2001-2012 (2000-2014 for CMIP6-historical and 2086-2100 for CMIP6-SSPs), σ_{n-1} is the standard deviation of the sample. Also, y_n is the reduced mean and S_n is the reduced standard deviation, which for n = 11 years (since we are calculating S_r in a hydrological year (i.e., simulation starts mid-year), we therefore lose one year) is equal to 0.4996 and 0.9676, respectively; and 0.5100 and 1.0095 for n = 14 years, respectively (Gumbel, 1958).

We later compare the S_r estimates derived from daily and monthly empirical estimates (Eq. 1 and 2) in Supplementary Figure 8 to evaluate uncertainty.

Supplementary Figures

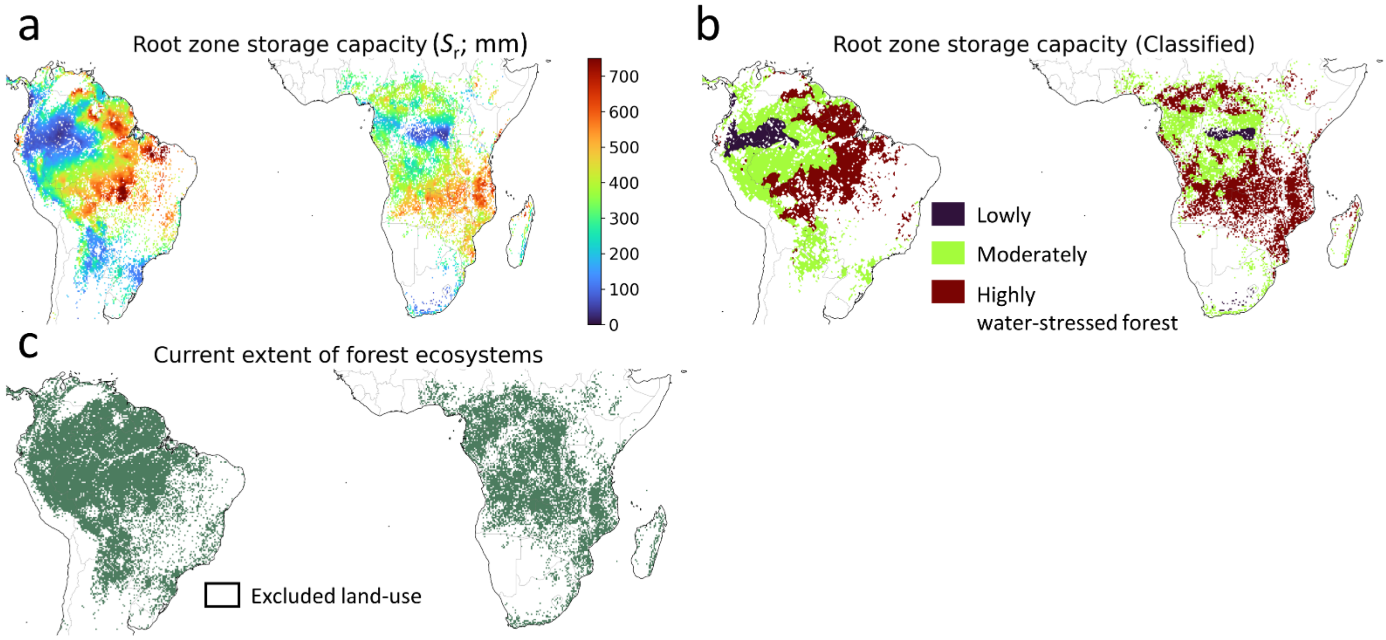

Supplementary Figure 1 | Root zone storage capacity (S_r) and extent of forest ecosystems. (**a**) Root zone storage capacity (S_r) based on empirical estimates of precipitation and evaporation (2001-2012). (**b**) Root zone storage capacity (S_r)-based classification of forest ecosystems (see methods). (**c**) This study's extent of tropical forests is based on the Global landcover classification – Globcover (GlobCover land-use map, 2022).

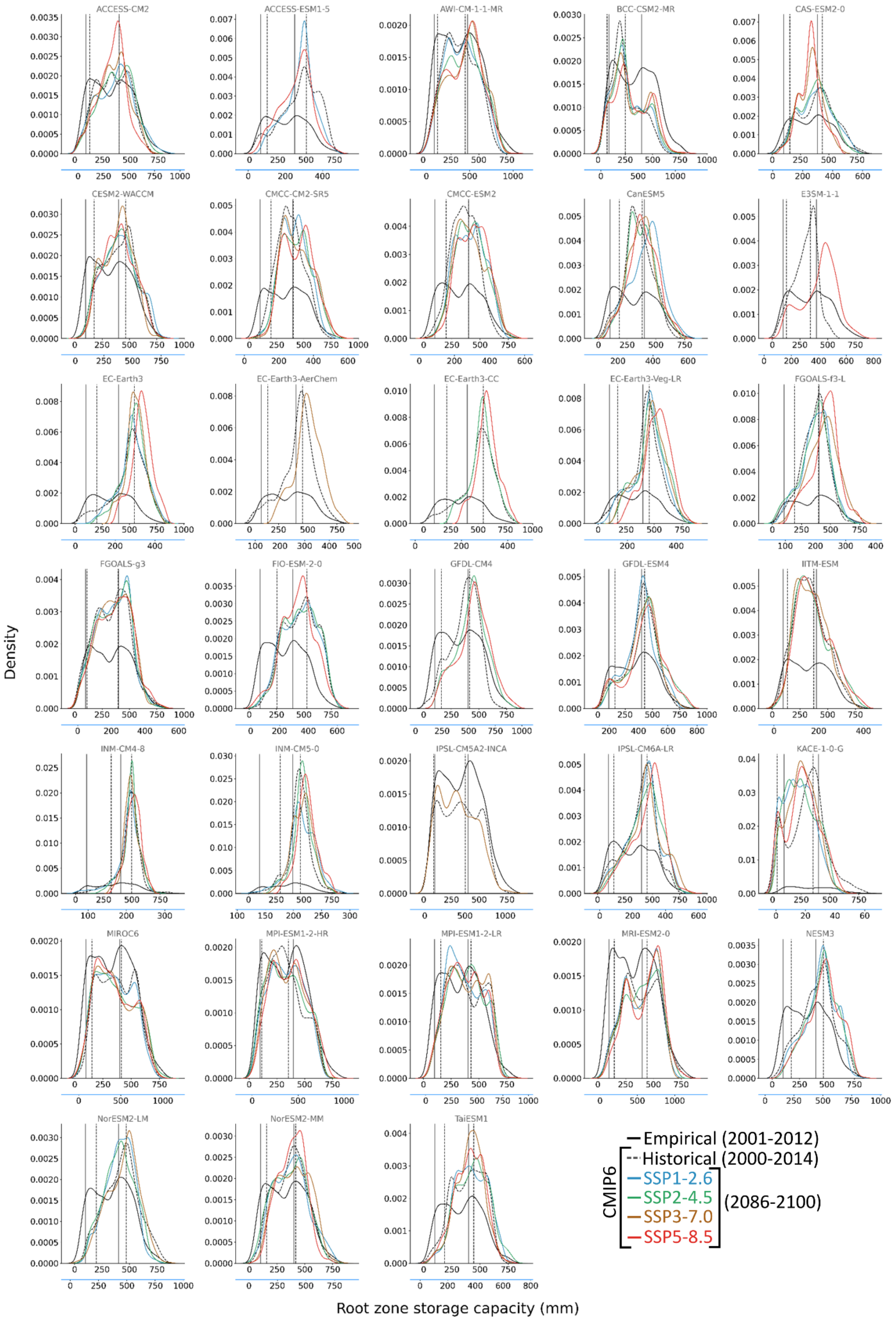

Supplementary Figure 2 | Frequency distribution of empirical- vs CMIP6-derived root zone storage capacity (S_r) for South America. Solid vertical lines represent lower and upper S_r threshold, whereas dotted vertical lines represent percentile-equivalent lower and upper S_r threshold based on bias correction (Fig. 1a,b and Supplementary Table 1; see methods). The top x-axis (in black) is for empirical S_r estimates, whereas the bottom x-axis (in blue) is for CMIP6 S_r estimates.

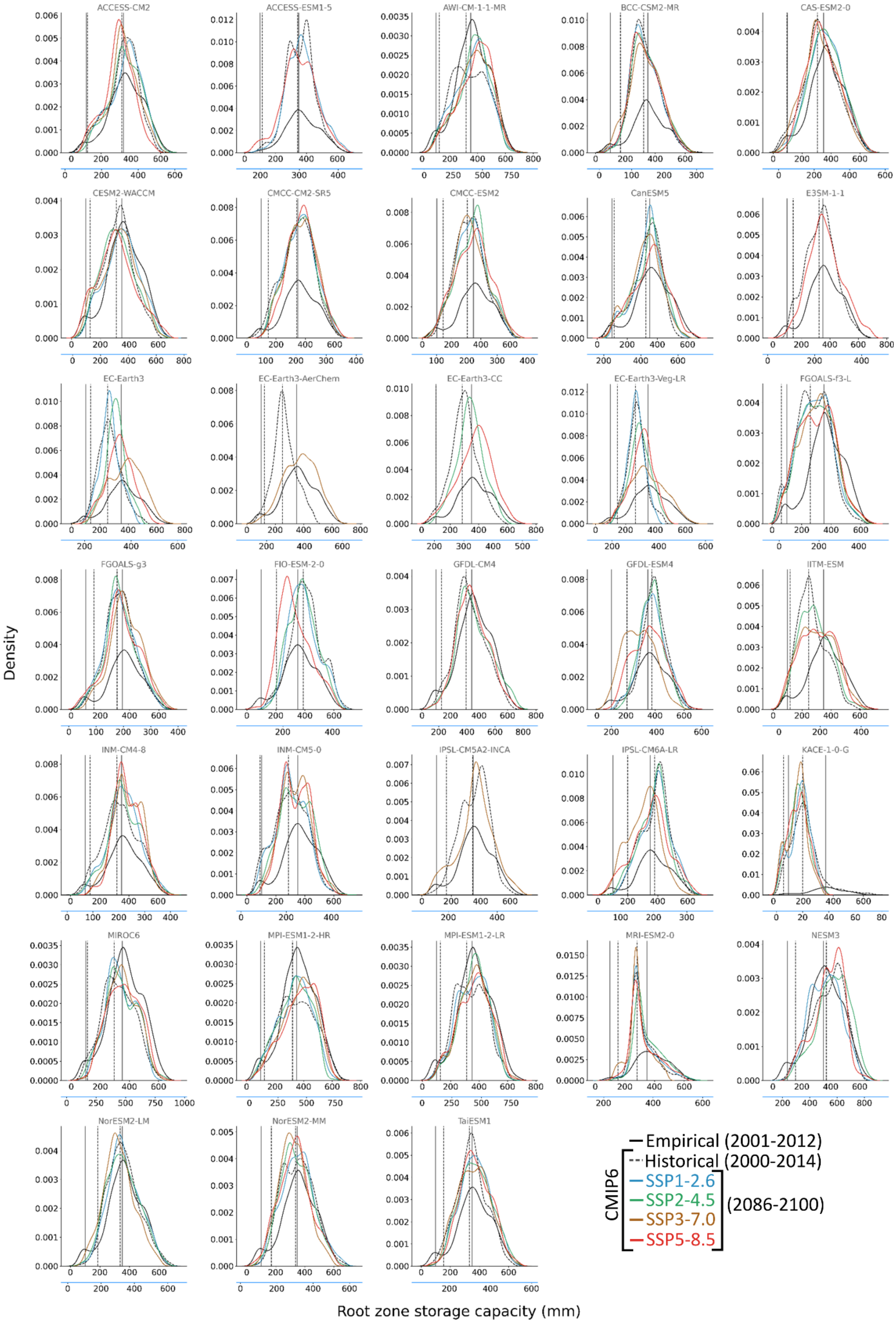

Supplementary Figure 3 | Frequency distribution of empirical- vs CMIP6-derived root zone storage capacity (S_r) for Africa. Same as Supplementary Fig. 2, but for Africa.

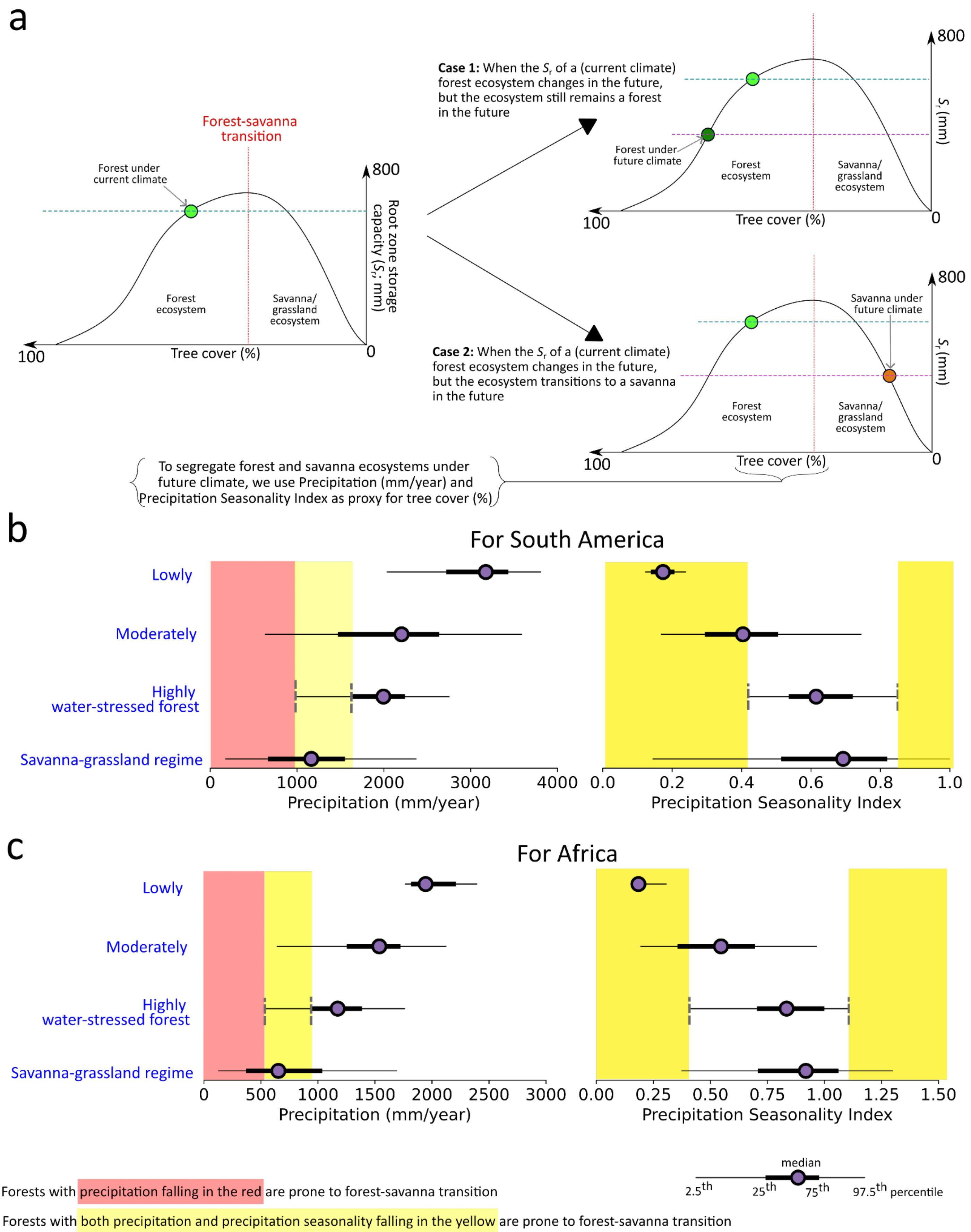

Supplementary Figure 4 | Forest and savanna segregation (i.e., revising forest classification) based on precipitation and precipitation seasonality using the current hydroclimate estimates (empirical; 2001-2012). (a) Illustration of cases where forest ecosystem's S_r changes under the future climate. (b,c) Dashed lines define the quantitative estimate of the threshold (for more details, refer to the methods and Fig. 1). Precipitation seasonality index is calculated using

Walsh and Lawler (1981) $\left(\frac{1}{R_i}\sum_{n=1}^{12}\left|X_{in}-\frac{R_i}{12}\right|\right)$. Here, R_i and X_{in} denote the total annual precipitation and monthly precipitation for the month *n*, respectively.

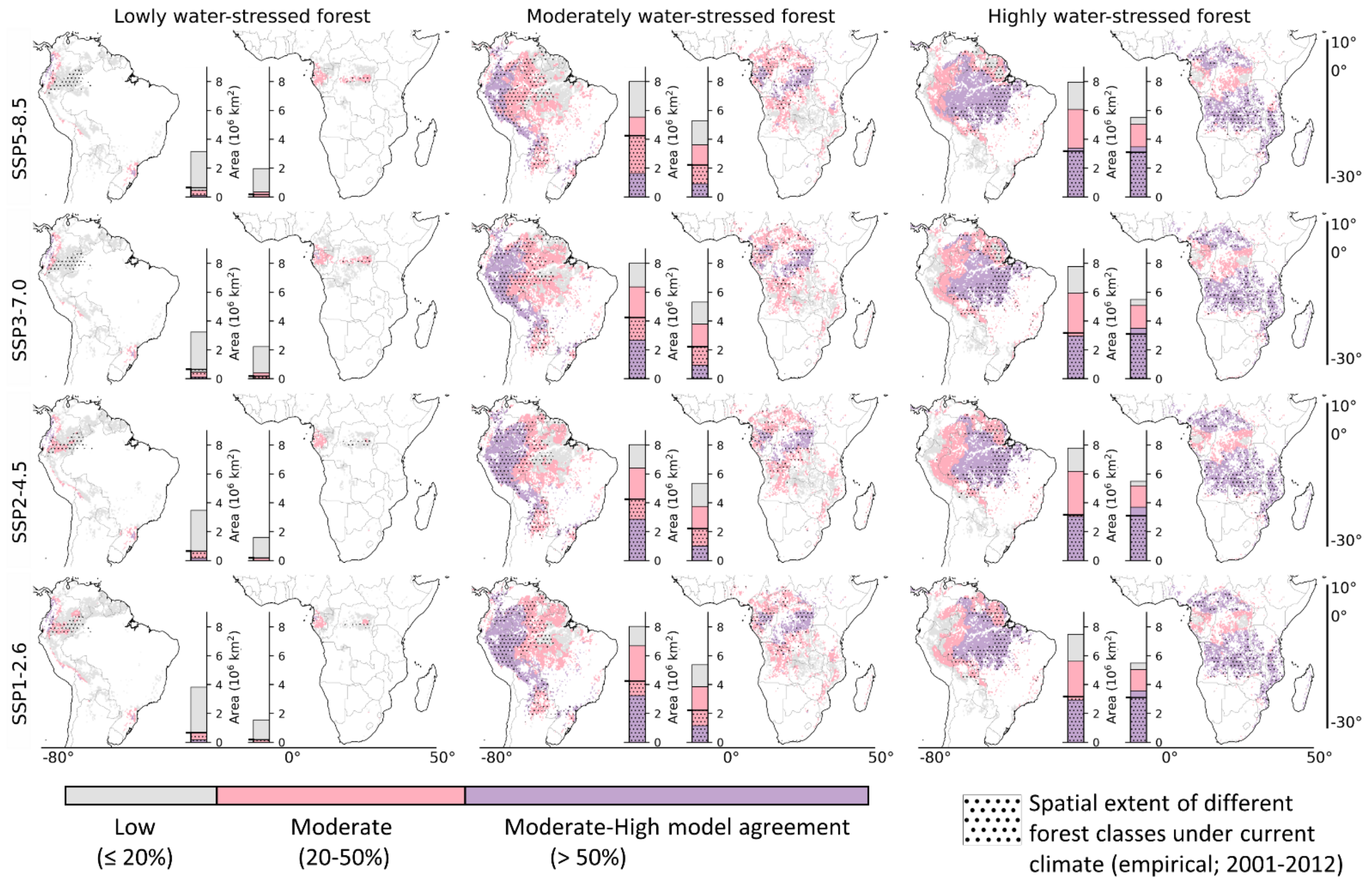

Supplementary Figure 5 | State of the tropical forests under different SSP scenarios (2086-2100) w.r.t current climate (empirical; 2001-2012). We aggregate the future state of the forest ecosystems by classifying the results of all CMIP6-SSPs into low (≤ 20%), moderate (20-50%) and moderate-high (> 50%) model agreement. Bar plots within each subplot – left for South America and right for Africa – correspond to the synthesised area of model agreement. Pixels with a hydroclimate similar to the savanna-grassland regime under the current climate (empirical; 2001-2012) are excluded from this analysis (example shown in black in Supplementary Fig. 7).

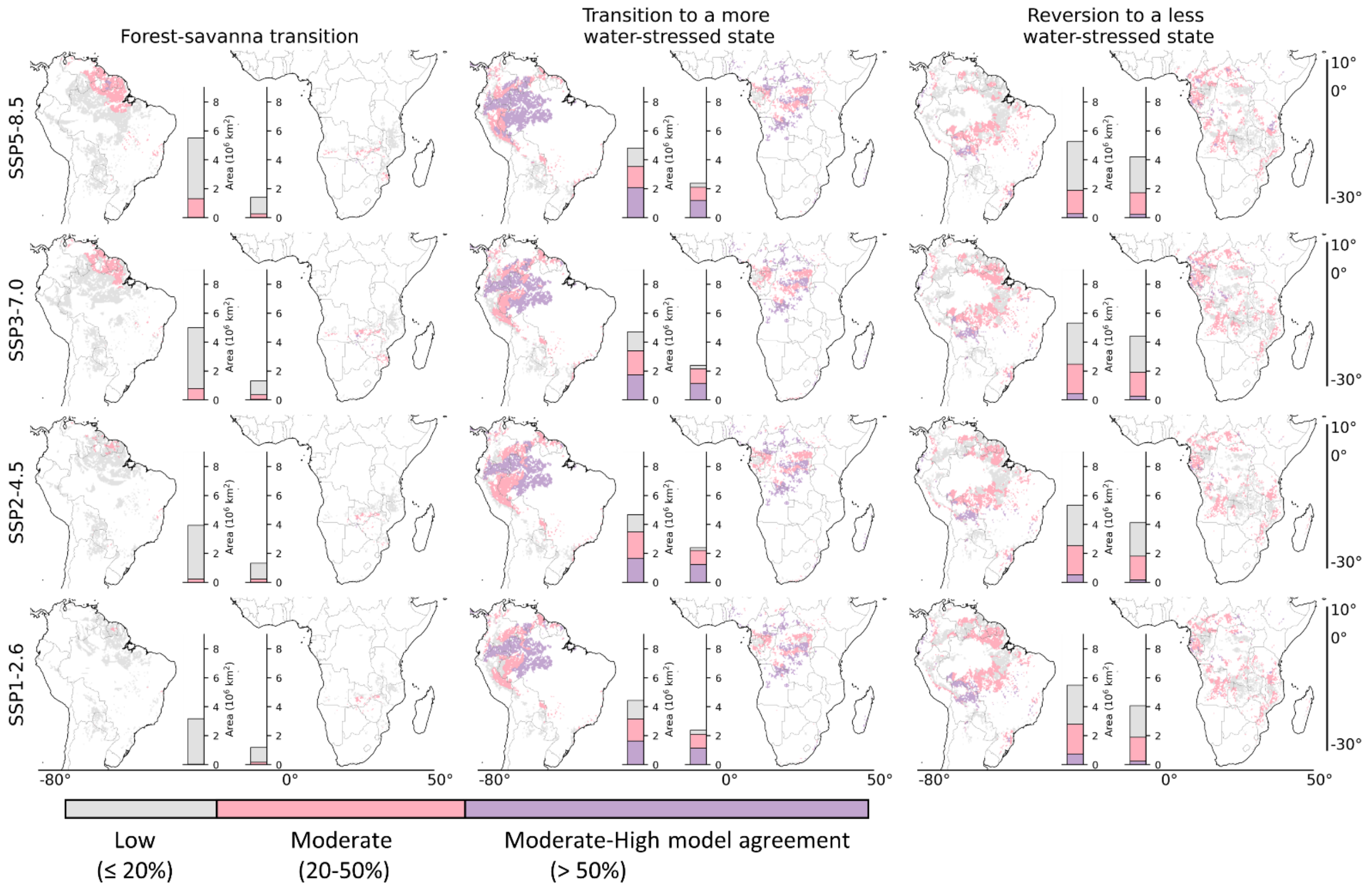

Supplementary Figure 6 | Extent of forest transitions under different SSP scenarios (2086-2100) w.r.t current climate (empirical; 2001-2012). Here, the transitions are derived based on the state of the forests under the current climate (empirical; 2001-2012). Bar plots within each subplot – left for South America and right for Africa – correspond to the synthesised area of model agreement. Synthesis for this figure is provided in Figs. 2 and 3.

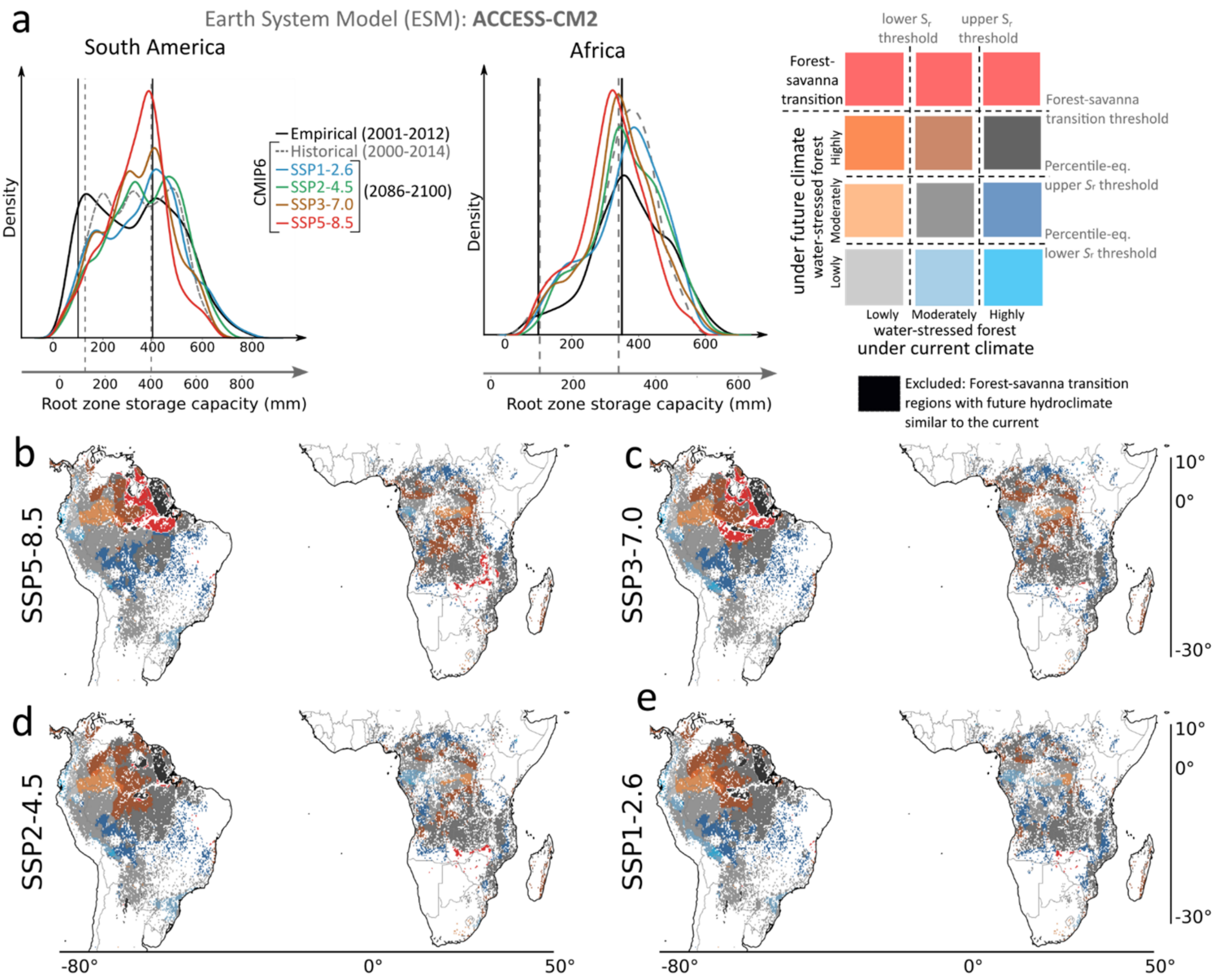

Supplementary Figure 7 | Exemplifying the methodological framework for projecting the future transitions in the tropical forests (by the end of the 21st century) based on the 'Australian Community Climate and Earth System Simulator coupled model (ACCESS-CM2)'. (a) Frequency density distribution of empirical (based on empirical *P* and *E* estimates) and CMIP6-derived S_r (based on *P* and *E* estimates from ACCESS-CM2 simulations) for South America and Africa. Based on empirical S_r classification, the solid vertical lines mark the lower (100 mm for both South America and Africa) and upper (400 mm for South America and 350 mm for Africa) S_r thresholds. Whereas dotted vertical lines demarcate the lower (116.58 mm for South America and 121.11 mm for Africa) and upper (409.90 mm for South America and 310.66 mm for Africa) percentile-equivalent S_r thresholds for CMIP6-historical (i.e., 2000-2014) models. We analyse forest-savanna transitions based on Supplementary Fig. 4. **(b-e)** Forests classification and transitions under different SSP scenarios, based on the comparison between empirical and CMIP6-SSPs (i.e., 2086-2100) derived forest classes (legend in the top-right corner). The white regions correspond to excluded landcover, including water and human-influenced land use (Supplementary Fig. 1c).

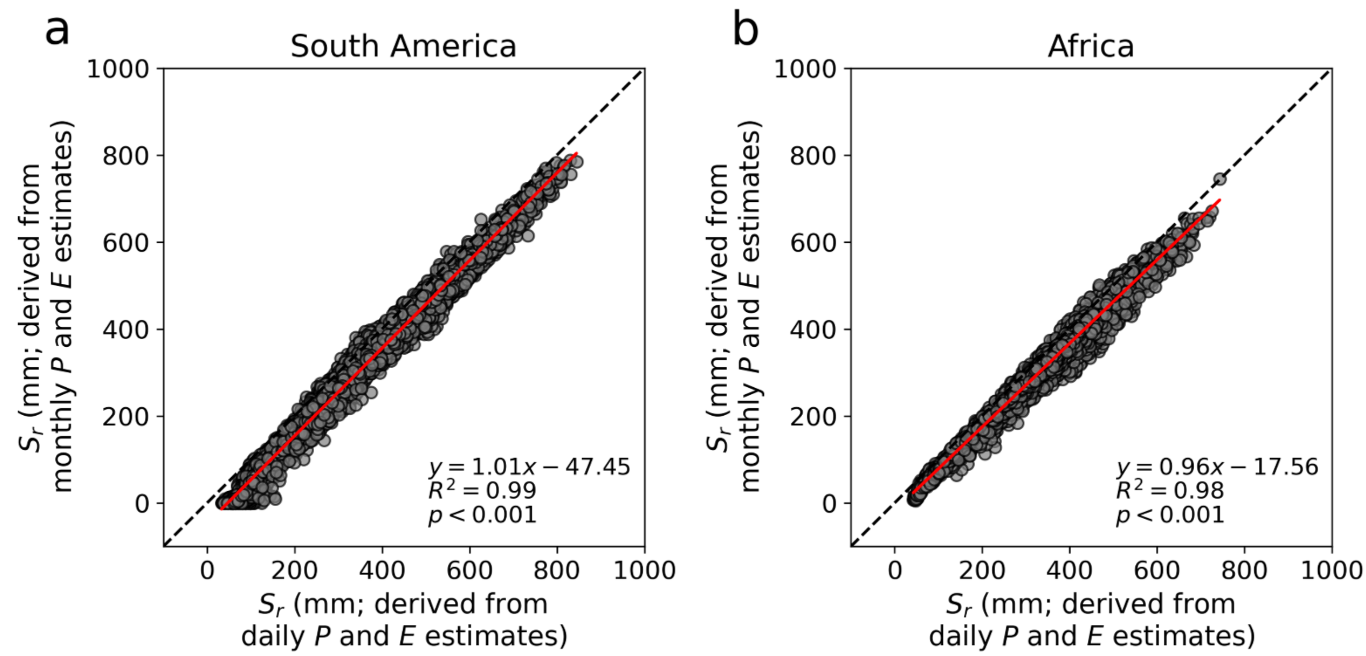

Supplementary Figure 8 | Comparing root zone storage capacity (S_r) based on daily and monthly estimates of precipitation (P) and evaporation (E) (both empirical; 2001-2012) for South America and Africa. Here, the regression line is represented in red, whereas the black dashed line represents the 1:1 between daily and monthly P and E derived S_r.

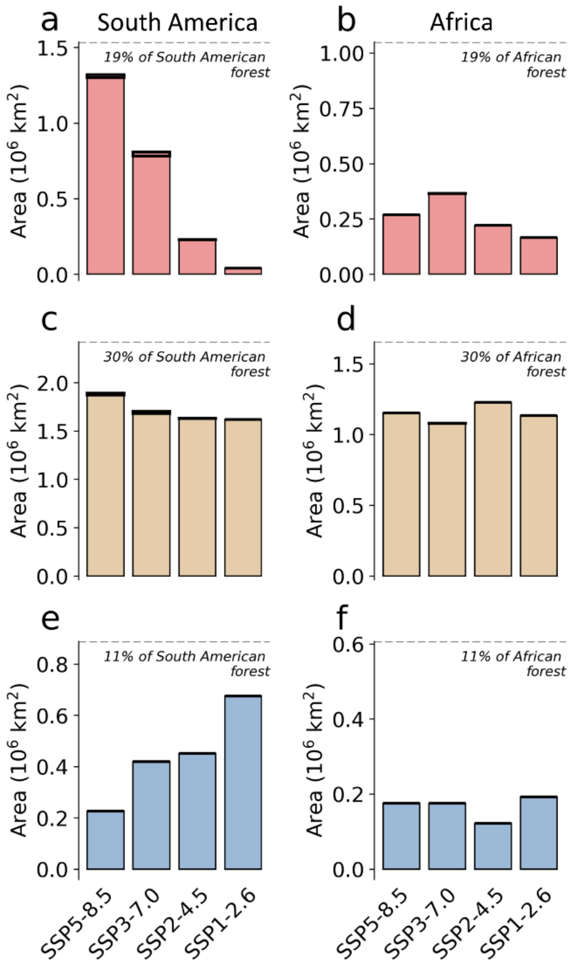

Supplementary Figure 9 | Comparing the forest transitions under different SSP scenarios. Same as Fig. 2, quantifying (**a,b**) forest-savanna transition, (**c,d**) forests' that transition to a more water-stressed state and **(e,f)** revert to a less water-stressed state for South America (total forest area 8.08 × 106 km^2) and Africa (total forest area 5.52 × 106 km^2). However, the model agreement is >20% for the forest-savanna transition, and for the other two transitions, the model agreement is >50%. These quantifications show the forests' state changes based on empirical-current (2001-2012) and future (2086-2100) climate conditions. For each transition, the total area of spatial overlap with other transitions under the same SSP scenario is highlighted with thick black bars.

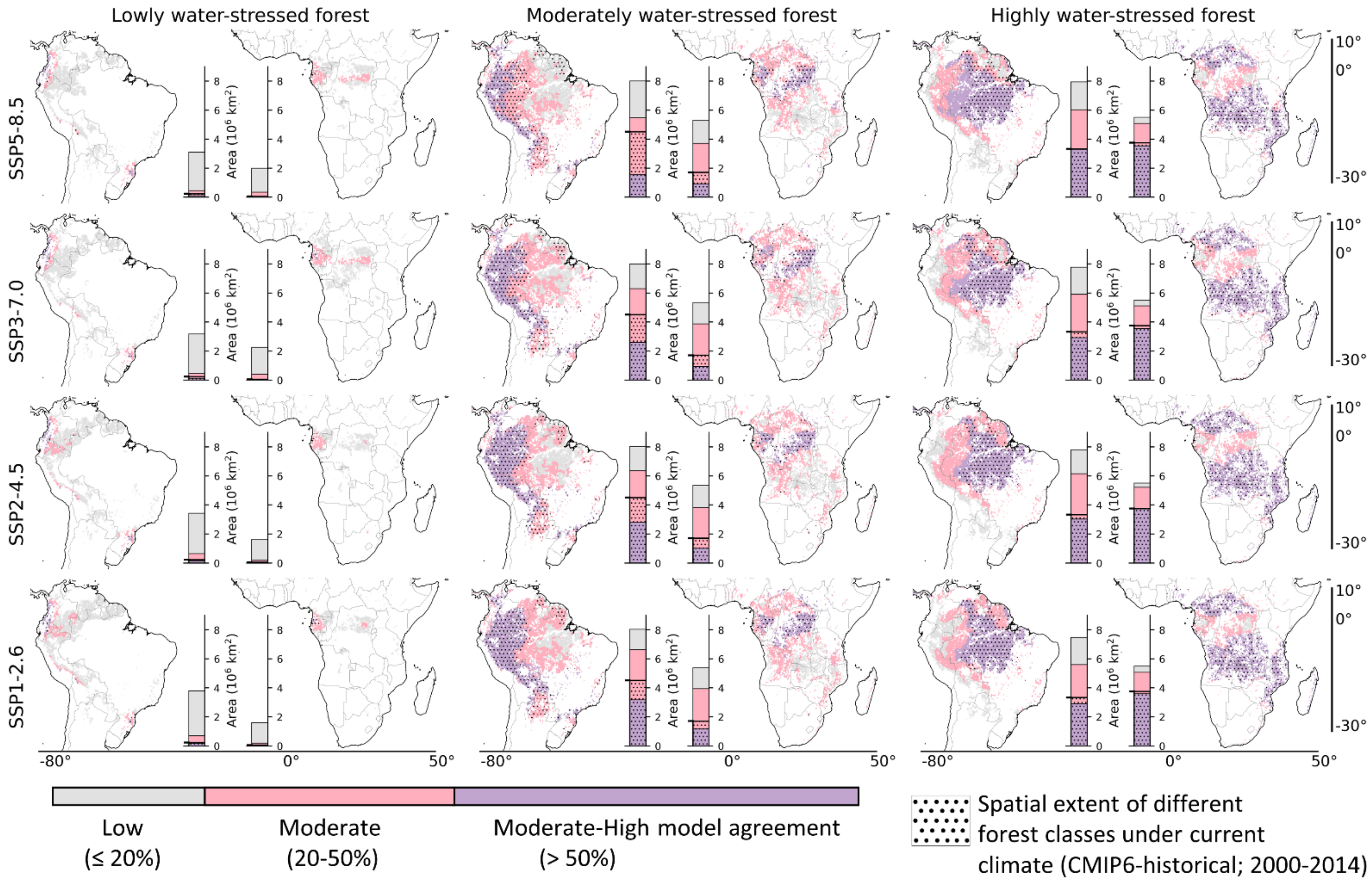

Supplementary Figure 10 | State of the tropical forests under different SSP scenarios (2086-2100) w.r.t current climate (CMIP6-historical; 2000-2014). Same as Fig. 5, but compared to CMIP-historical estimates (2000-2014).

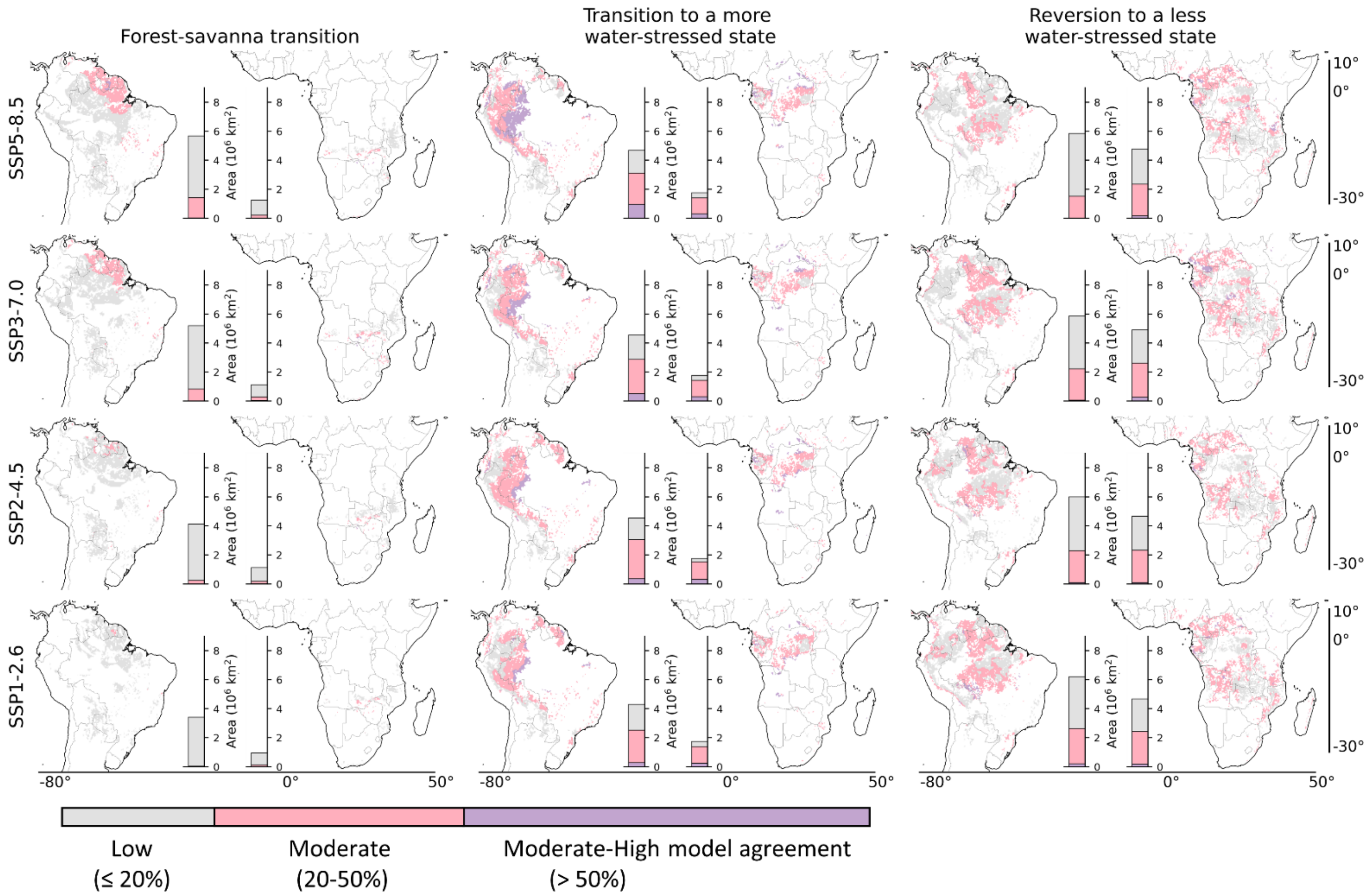

Supplementary Figure 11 | Extent of forest transitions under different SSP scenarios (2086-2100) w.r.t current climate (CMIP-historical; 2000-2014). Same as Fig. 6, but compared to CMIP-historical estimates (2000-2014).

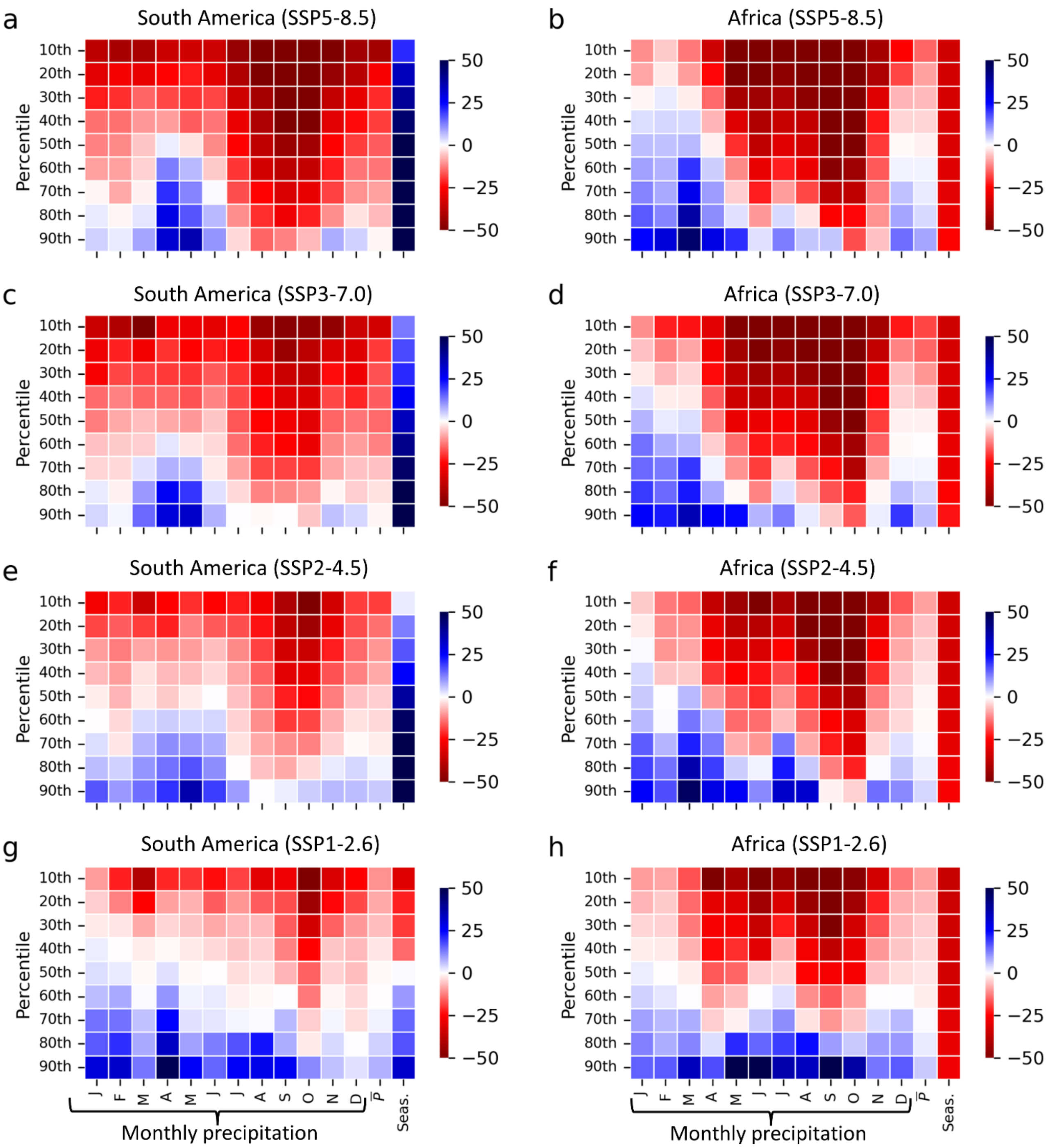

Supplementary Figure 12 | Comparing hydroclimatic changes between current and future climate for forest-savanna transition regions. The extent of forest-savanna transition can be referred from Fig. 3. Since there is considerable variability between empirical and CMIP6-model estimates, we directly compare current (CMIP6-historical; 2000-2014) hydroclimate with the future (CMIP6-SSPs; 2086-2100) using estimates from the ESMs. Here, we focus on monthly precipitation, mean annual precipitation ($\overline{P}$) and precipitation seasonality (Seas.). The percentile is calculated across different ESMs. The colour bar represents the % change in variables with respect to the current climate (2000-2014).

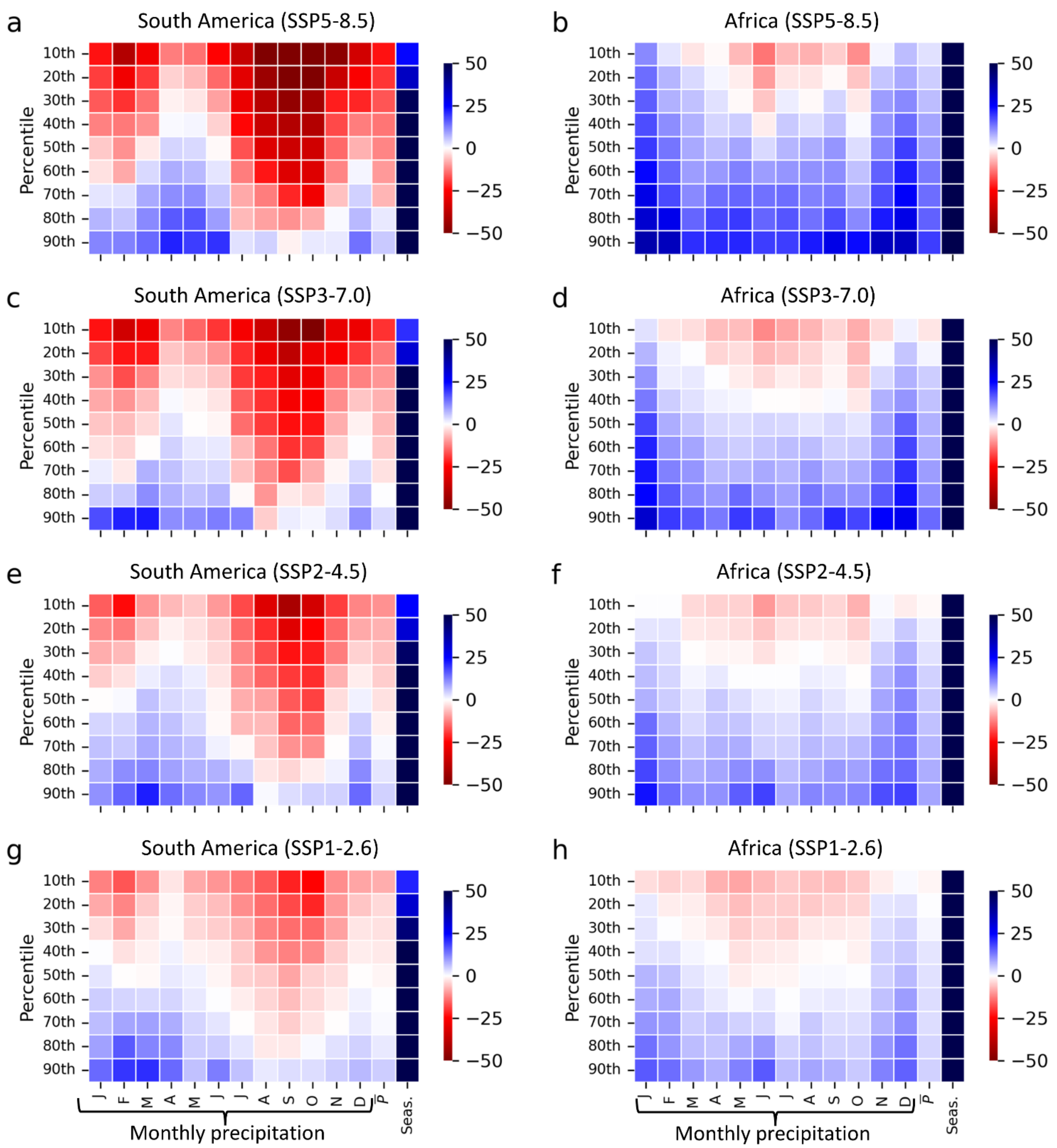

Supplementary Figure 13 | Comparing hydroclimatic changes between current and future climate for forests' that transition to a more water-stressed state. Same as Supplementary Fig. 12, but for forest ecosystems that transition to a 'more' water-stressed state.

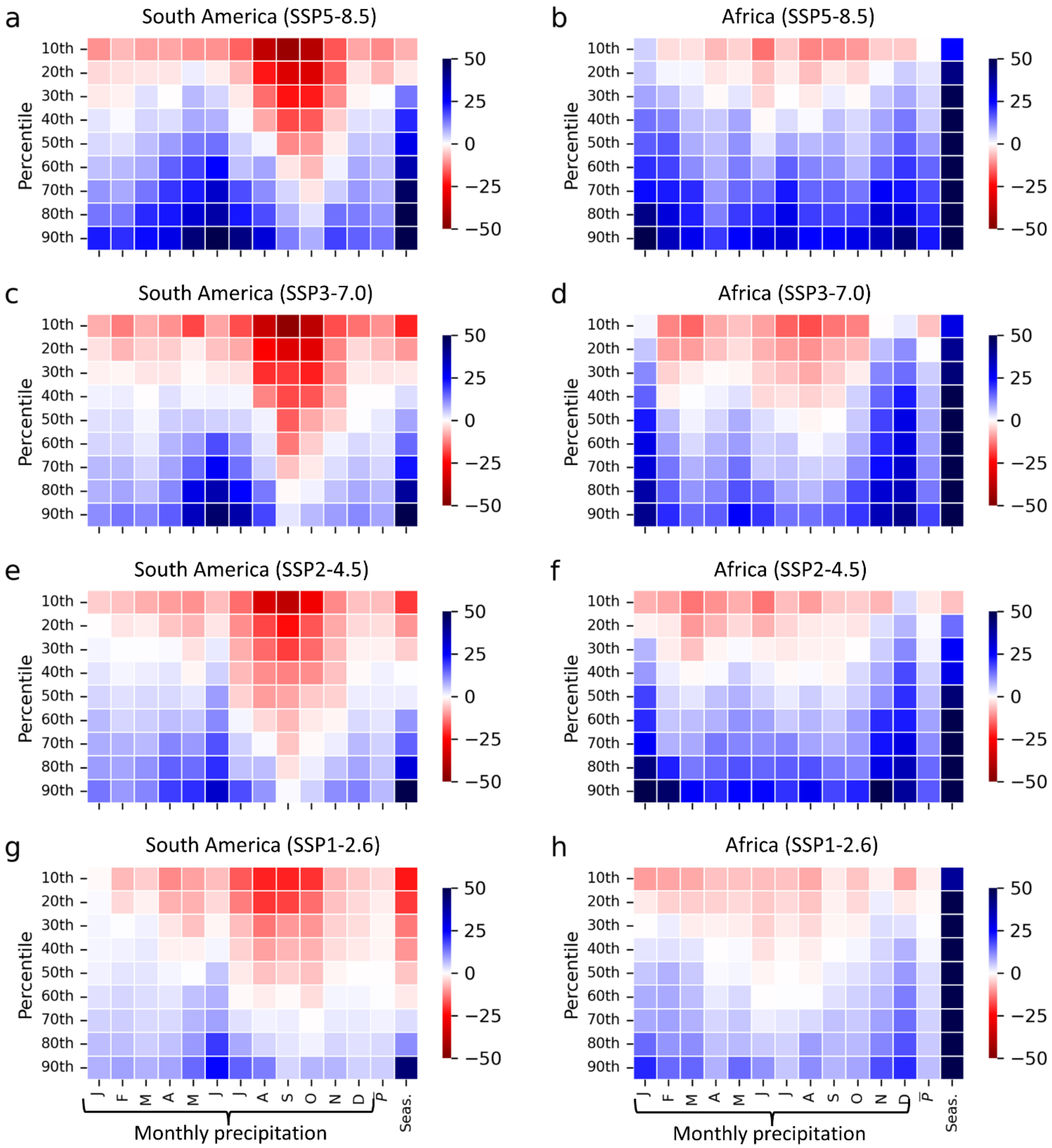

Supplementary Figure 14 | Comparing hydroclimatic changes between current and future climate for forests' that revert to a less water-stressed state. Same as Supplementary Fig. 12, but for forest ecosystems that revert to a 'less' water-stressed state.

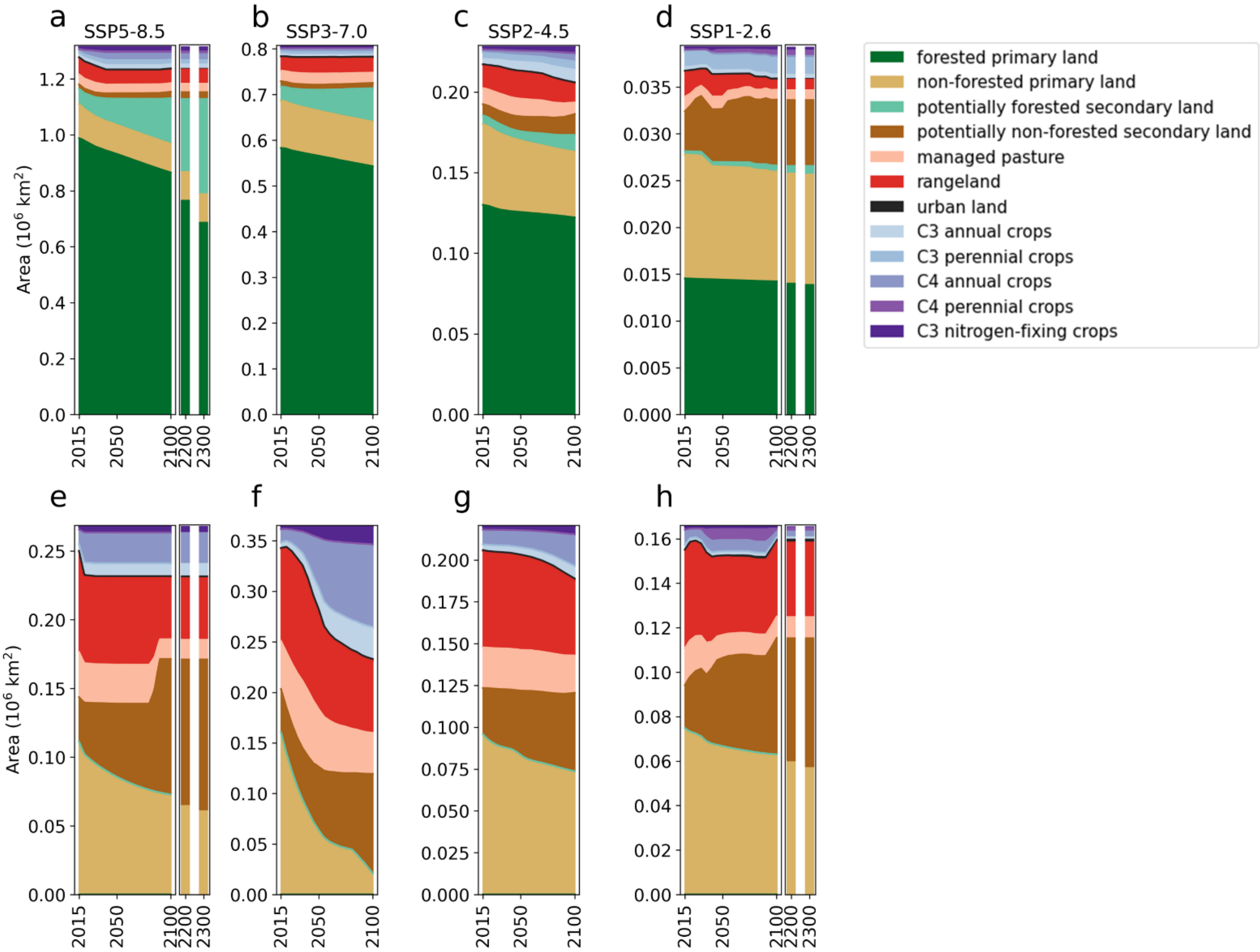

Supplementary Figure 15 | Comparing forest-savanna transitions with prescribed land-use in ESMs. Here, we compare Integrated Assessment Models (IAMs) derived land-use (also referred to as 'land-use harmonisation')(Hurtt et al., 2020) with projected forest-savanna transitions (extent of transition defined in Fig. 3). We analyse the land-use between 2015-2100 and the median between 2186-2200 and 2286-2300 for (**a-d**) South America and (**e-h**) Africa. Here, ‘primary’ land-use refers to the regions that have never been impacted by human influence since the start of the simulation. Note that extended prescribed harmonised land-use data (2100-2300) is only available for SSP5-8.5 and SSP1-2.6, and therefore is not analysed for the other two SSP scenarios.

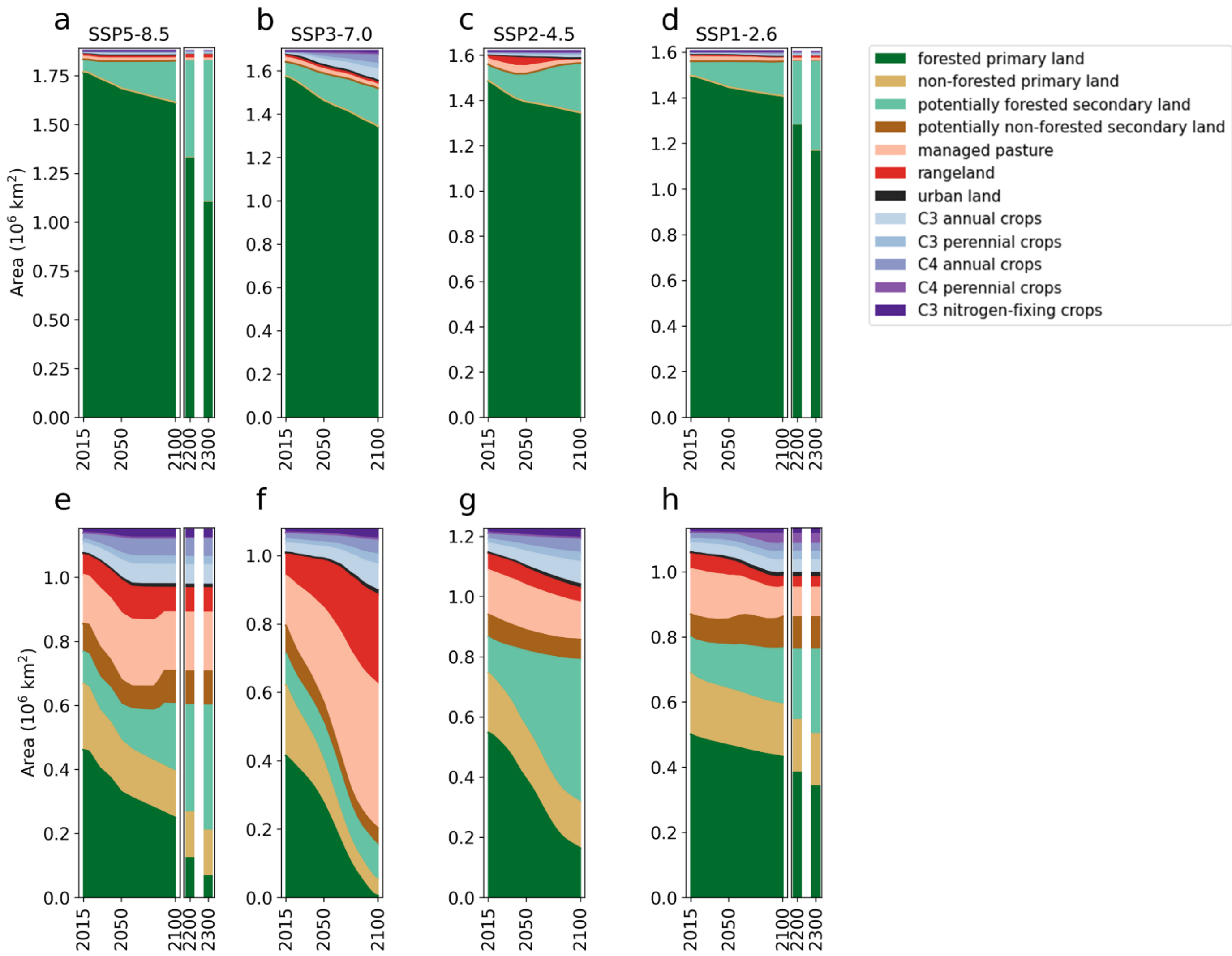

Supplementary Figure 16 | Comparing forests that transition to a more water-stressed state with prescribed land-use in ESMs. Same as Supplementary Fig. 15, but for the forest that transition to a more water-stressed state.

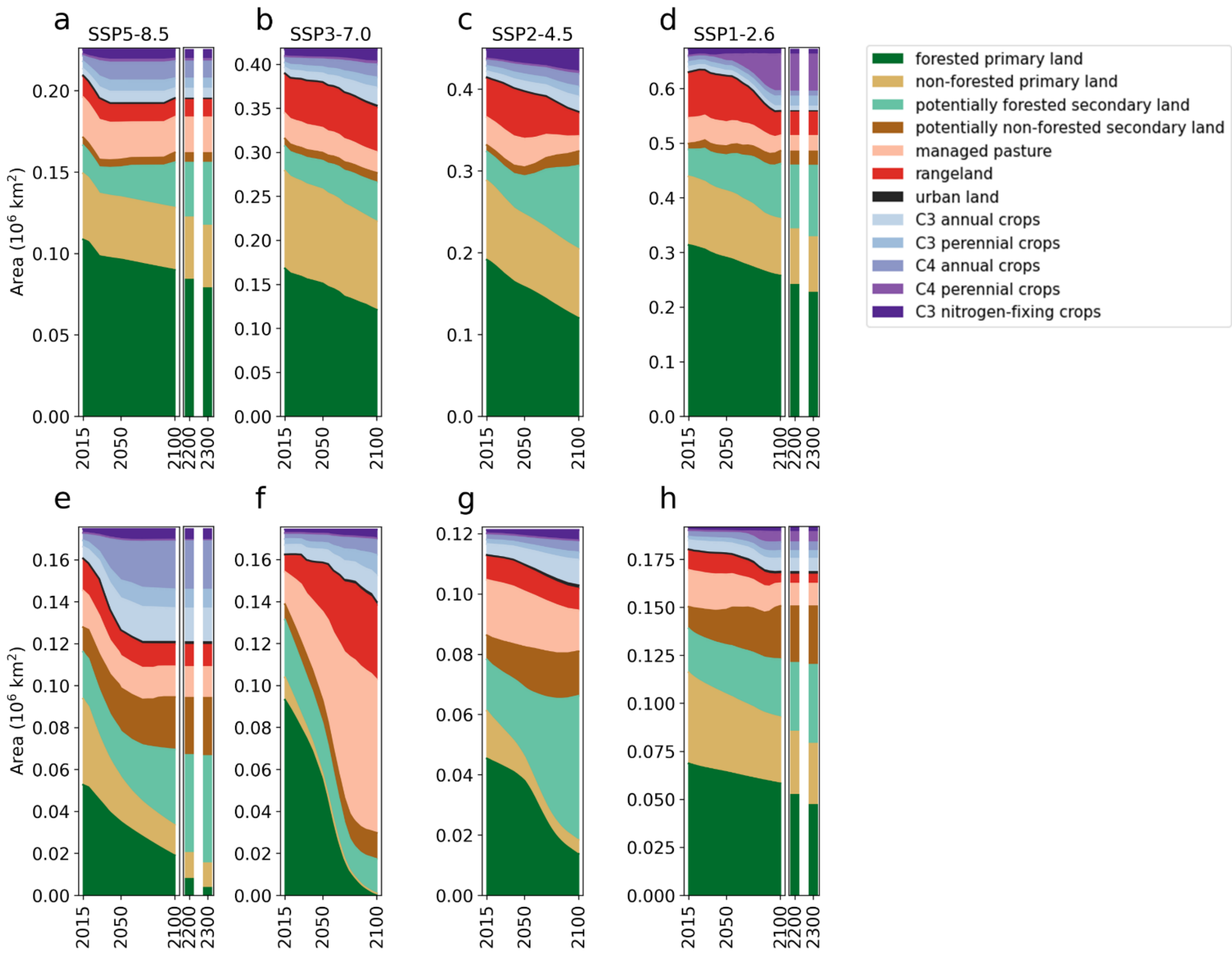

Supplementary Figure 17 | Comparing forests that revert to a less water-stressed state with prescribed land-use in ESMs. Same as Supplementary Fig. 15, but for forests that transition to a less water-stressed state.

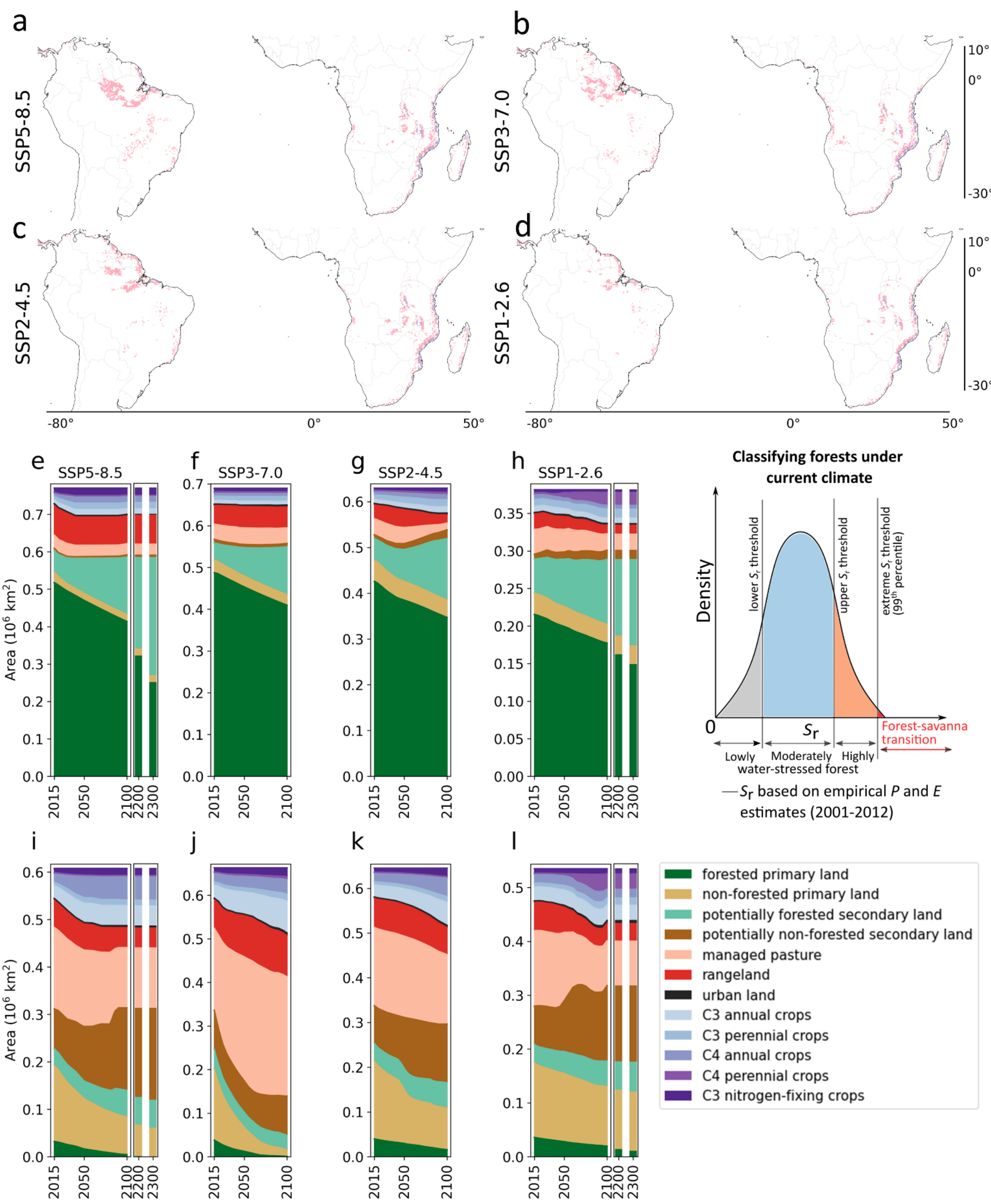

Supplementary Figure 18 | Analysing and comparing (extreme value) forest-savanna transitions with prescribed land-use in ESMs. One can argue that mass-balance based S_r might over-estimate forests if forest ecosystems are not able to maintain their above-ground structure at high S_r (i.e., unrealistic S_r from a plant's perspective). Considering forest-savanna transition thresholds defined in Fig. 4, here we additionally assumed that regions that exceed the 99th percentile S_r are also prone to a forest-savanna transition. (**a-d**) These additional regions (excluding those already defined in Fig. 3) are evaluated using bias-corrected values for all ESMs under different SSP scenarios (same as Fig. 1). (**e-l**) Same as Supplementary Fig. 15, but only for the additional regions in a-d (see methods for more details). These additional transition regions are not included in the analyses presented in the Figs. 2 and 3.

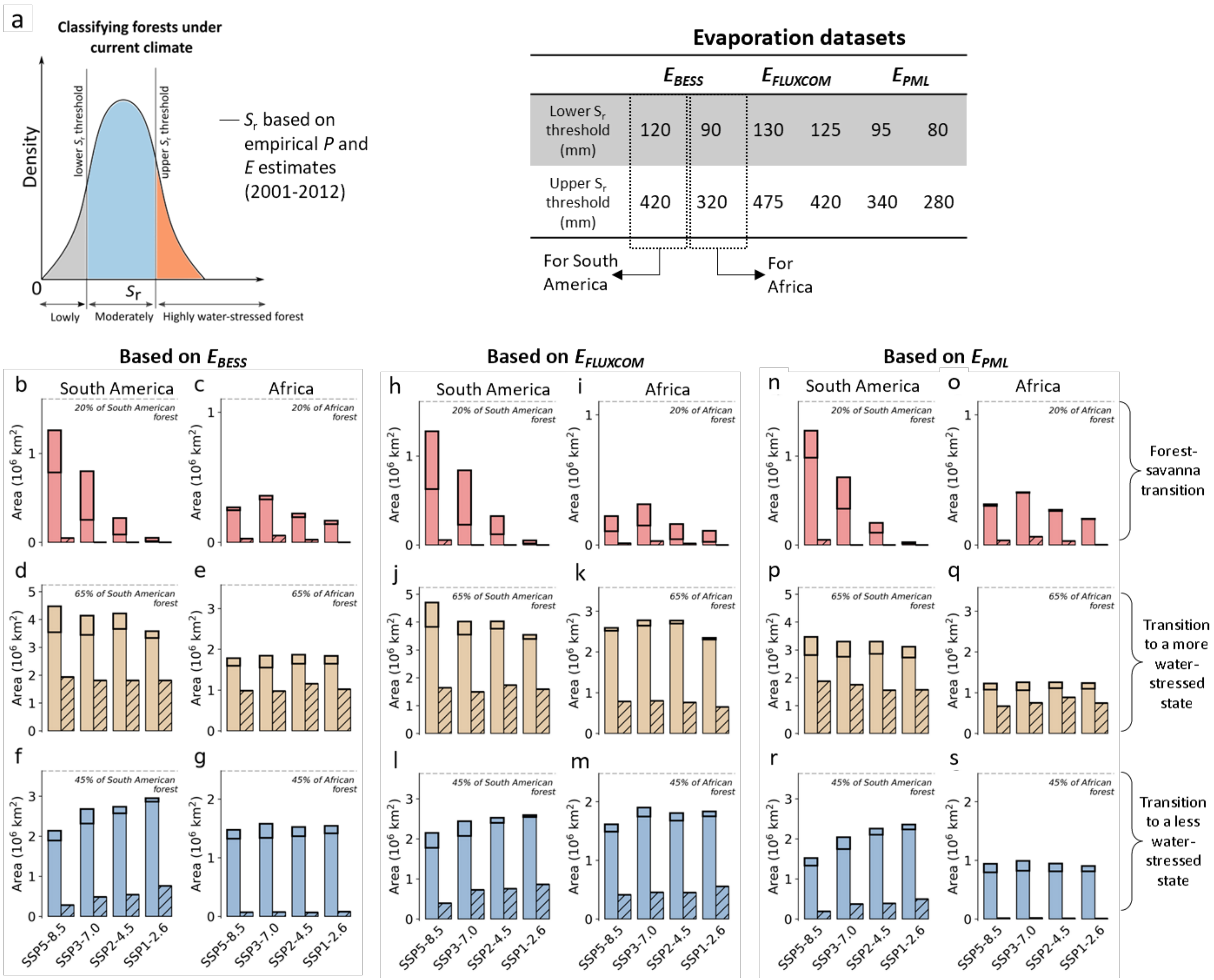

Supplementary Figure 19 | Sensitivity analysis with root zone storage capacity (S_r) forest classification thresholds derived using different evaporation products. (**a**) For this sensitivity analysis, we estimate forest classification thresholds based on evaporation estimates of (b-g) BESS, (h-m) FLUXCOM and (n-s) PML for South America and Africa. Figure legend remain same as Fig. 2.

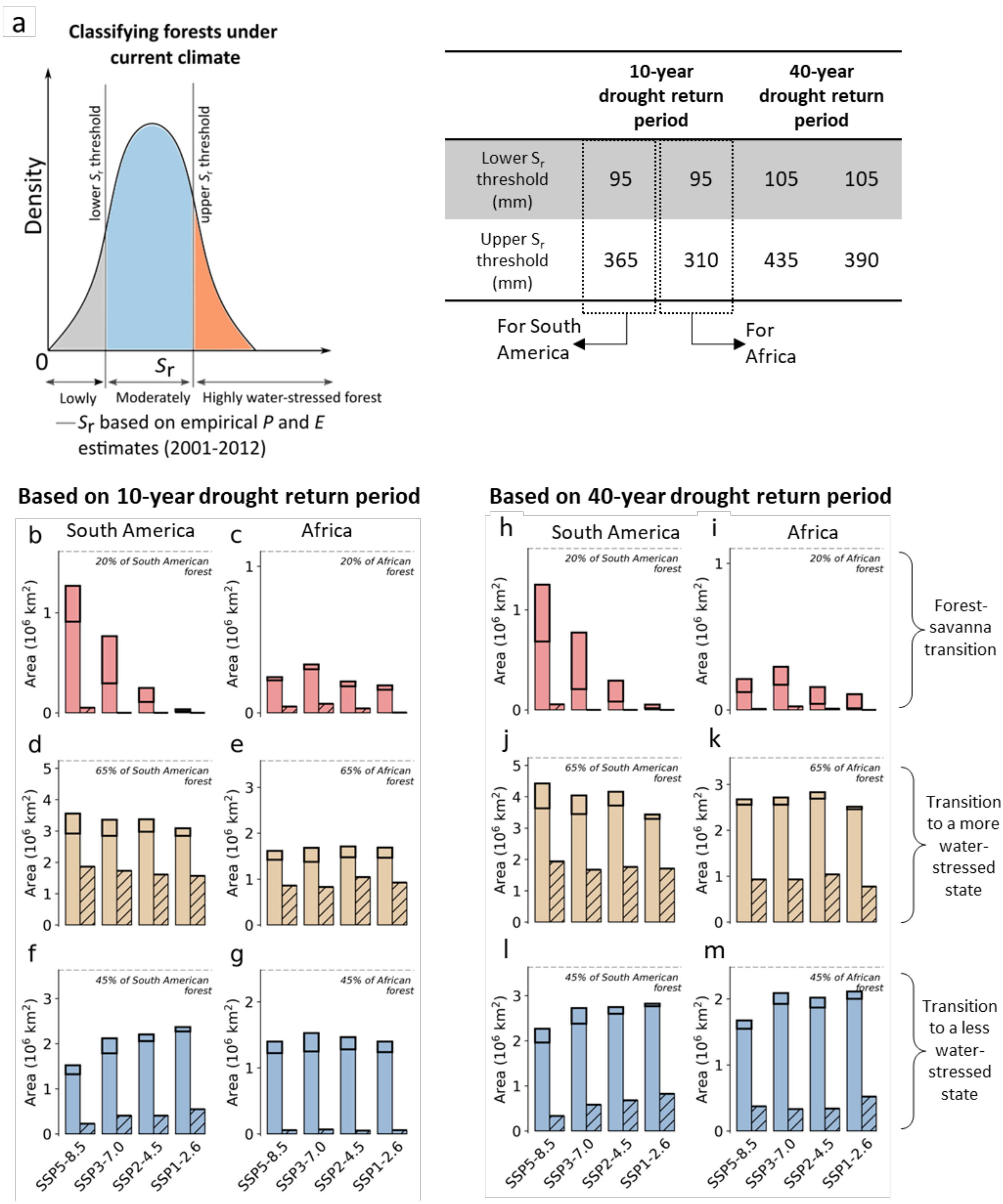

Supplementary Figure 20 | Sensitivity analysis with root zone storage capacity (S_r) forest classification thresholds derived at different drought return periods. (**a**) For this sensitivity analysis, we estimate forest classification thresholds based on (b-g) 10- and (h-m) 40-year drought return period for South America and Africa. Figure legend remain same as Fig. 2.

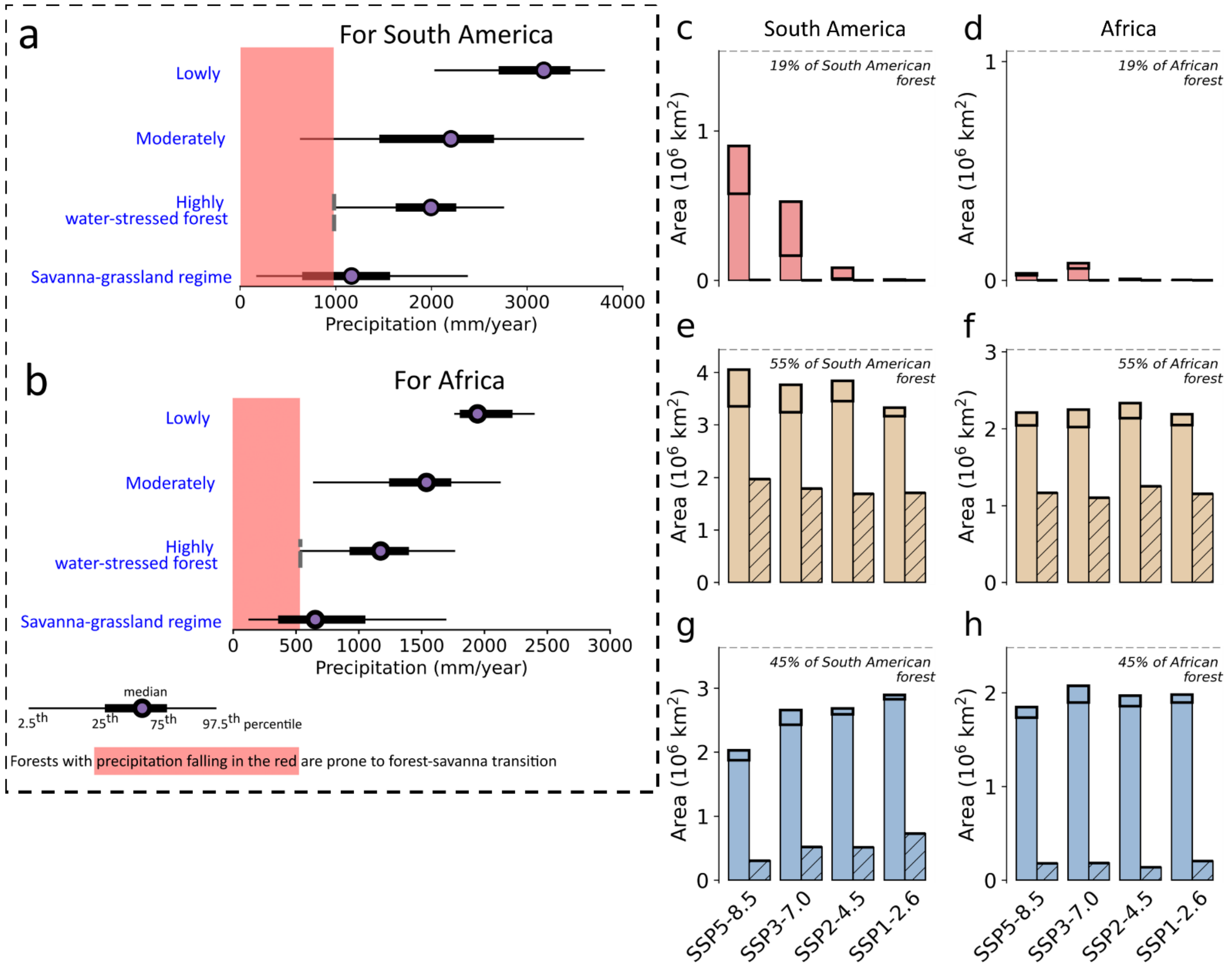

Supplementary Figure 21 | Sensitivity analysis with lower forest-savanna transition threshold. Same as Supplementary Fig. 19, but for this sensitivity analysis, (**a,b**) we decreased the forest-savanna transition threshold for South America and Africa (relative to Fig. 4). Figure legend remain same as Fig. 2.

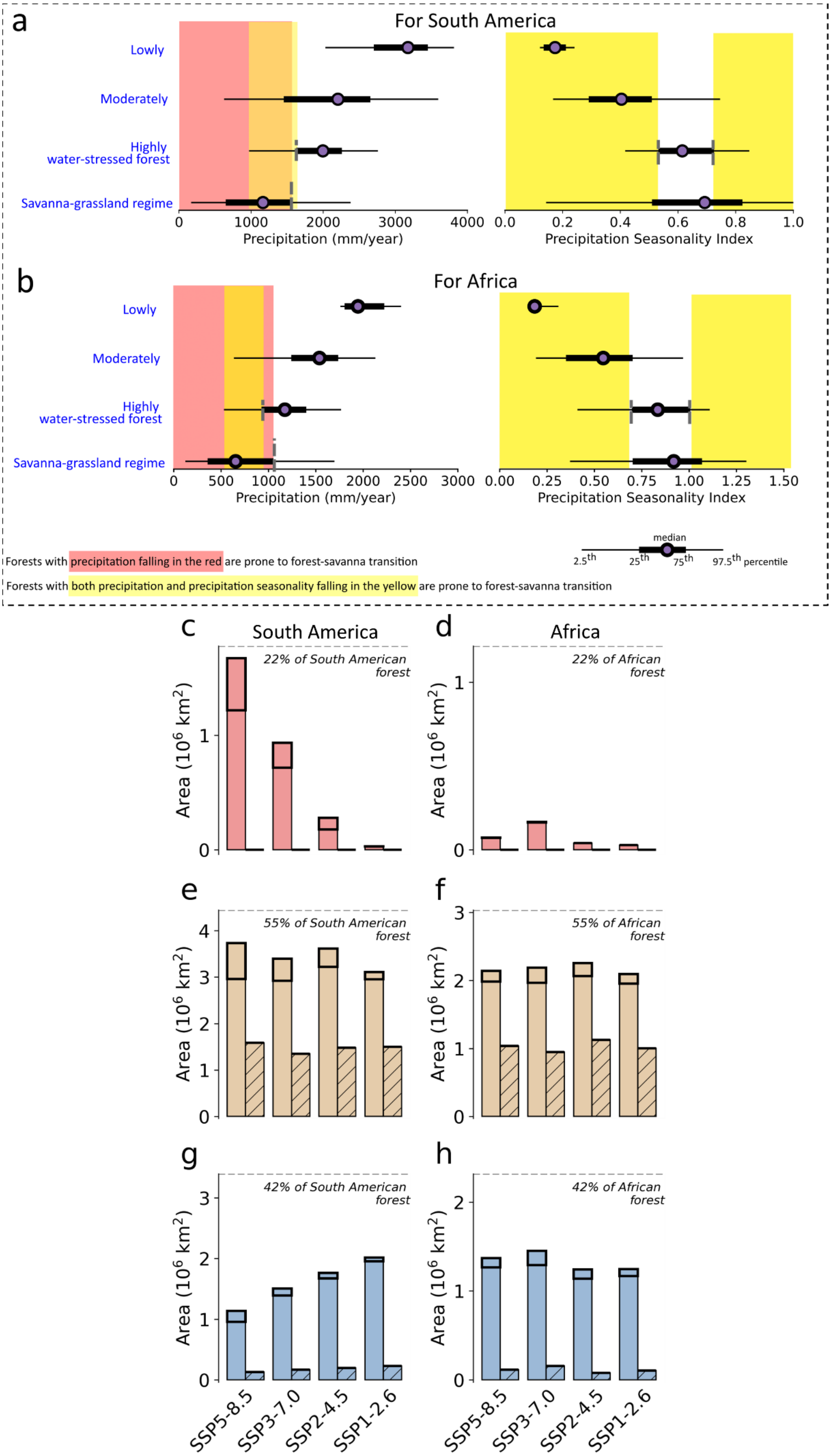

Supplementary Figure 22 | Sensitivity analysis with higher forest-savanna transition threshold. Same as Supplementary Fig. 19, but for this sensitivity analysis, (**a**,**b**) we increased the forest-savanna transition threshold for South America and Africa (relative to Fig. 4). Figure legend remain same as Fig. 2.

Supplementary Tables

Supplementary Table 1 | Overview of analysed Earth System Models (ESMs). Here, '1' represents the analysed models, whereas '0' represents models excluded from this study due to data unavailability. All ESM estimates have a variable label 'r1i1p1f1' and are downloaded at a monthly timescale. Refer to Fig. 1 for more details.

							For South America (Lower S_r threshold = 100 mm; Upper S_r threshold = 400 mm)		For Africa (Lower S_r threshold = 100 mm; Upper S_r threshold = 350 mm)	
Institution	**ESM**	**Historical** (2000-2014)	**SSP1-2.6** (2086-2100)	**SSP2-4.5** (2086-2100)	**SSP3-7.0** (2086-2100)	**SSP5-8.5** (2086-2100)	**Percentile-eq. lower S_r threshold (mm)**	**Percentile-eq. upper S_r threshold (mm)**	**Percentile-eq. lower S_r threshold (mm)**	**Percentile-eq. upper S_r threshold (mm)**
CSIRO-ARCCSS	ACCESS-CM2	1	1	1	1	1	116.58	409.90	121.11	310.66
CSIRO	ACCESS-ESM1-5	1	1	0	0	1	95.73	314.00	206.08	295.56
AWI	AWI-CM-1-1-MR	1	1	1	1	1	127.05	446.71	121.61	354.32
BCC	BCC-CSM2-MR	1	1	1	1	1	93.55	348.75	67.83	134.38
CAS	CAS-ESM2-0	1	1	1	1	1	120.42	336.19	49.69	220.27
NCAR	CESM2-WACCM	1	1	1	1	1	164.95	445.45	129.92	316.43
CMCC	CMCC-CM2-SR5	1	1	1	1	1	155.17	288.22	110.77	204.21
CMCC	CMCC-ESM2	1	1	1	1	1	147.60	282.74	122.63	203.50
CCCMA	CanESM5	1	1	1	1	1	194.05	337.46	258.61	422.44
E3SM-PROJECT	E3SM-1-1	1	0	0	0	1	165.40	338.41	110.79	217.85
EC-EARTH-CONSORTIUM	EC-Earth3	1	1	1	1	1	109.69	295.35	220.38	297.82
EC-EARTH-CONSORTIUM	EC-Earth3-AerChem	1	0	0	1	0	148.24	290.57	190.16	283.32
EC-EARTH-CONSORTIUM	EC-Earth3-CC	1	0	1	0	1	133.02	295.08	212.84	291.76
EC-EARTH-CONSORTIUM	EC-Earth3-Veg-LR	1	1	1	1	1	140.76	287.43	219.32	298.82
CAS	FGOALS-f3-L	1	1	1	1	1	132.62	211.54	8.59	158.33
CAS	FGOALS-g3	1	1	1	1	1	50.59	237.41	87.84	175.73

FIO-QLNM	FIO-ESM-2-0	1	1	1	0	1	175.22	389.88	171.90	281.87
NOAA-GFDL	GFDL-CM4	1	0	1	0	1	236.71	503.84	234.74	392.20
NOAA-GFDL	GFDL-ESM4	1	1	1	1	1	218.29	448.12	264.17	378.16
CCCR-IITM	IITM-ESM*	1	0	1	1	1	61.79	178.84	53.05	143.62
INM	INM-CM4-8	1	1	1	1	1	160.64	213.78	87.85	193.70
INM	INM-CM5-0	1	1	1	1	1	176.90	211.89	81.61	208.74
IPSL	IPSL-CM5A2-INCA	1	0	0	1	0	108.53	518.70	195.46	298.38
IPSL	IPSL-CM6A-LR	1	1	1	1	1	81.03	286.70	121.64	201.10
NIMS-KMA	KACE-1-0-G	1	1	1	1	1	0.98	24.42	5.28	19.71
MIROC	MIROC6	1	1	1	1	1	162.82	512.90	194.18	405.90
MPI-M/DKRZ	MPI-ESM1-2-HR	1	1	1	1	1	107.09	402.43	125.14	379.69
MPI-M	MPI-ESM1-2-LR	1	1	1	1	1	150.71	442.32	153.40	379.91
MRI	MRI-ESM2-0	1	1	1	1	1	184.23	620.21	270.23	334.59
NUIST	NESM3	1	1	1	0	1	225.25	501.55	304.84	514.99
NCC	NorESM2-LM	1	1	1	1	0	228.73	499.49	183.81	312.88
NCC	NorESM2-MM	1	1	1	1	1	154.86	414.64	164.23	309.66
AS-RCEC	TaiESM1	1	1	1	1	1	183.25	392.83	173.93	297.18
	(Total)	**33**	**27**	**29**	**27**	**30**				

* IITM-ESM simulations are only available between 2015-2099, except for the SSP3-7.0 scenario, for which data is available between 2015-2098.

Supplementary Table 2 | Citations for CMIP6 datasets used in this study.

Institution	ESM	Historical	SSP1-2.6	SSP2-4.5	SSP3-7.0	SSP5-8.5
CSIRO-ARCCSS	**ACCESS-CM2**	Dix et al. (2019). CSIRO-ARCCSS ACCESS-CM2 model output prepared for CMIP6 CMIP historical. Earth System Grid Federation. doi:https://doi.org/10.22033/ESGF/CMIP6.4271 .	Dix et al. (2019). CSIRO-ARCCSS ACCESS-CM2 model output prepared for CMIP6 ScenarioMIP ssp126. Earth System Grid Federation. doi:https://doi.org/10.22033/ESGF/CMIP6.4319 .	Dix et al. (2019). CSIRO-ARCCSS ACCESS-CM2 model output prepared for CMIP6 ScenarioMIP ssp245. Earth System Grid Federation. doi:https://doi.org/10.22033/ESGF/CMIP6.4321 .	Dix et al. (2019). CSIRO-ARCCSS ACCESS-CM2 model output prepared for CMIP6 ScenarioMIP ssp370. Earth System Grid Federation. doi:https://doi.org/10.22033/ESGF/CMIP6.4323 .	Dix et al. (2019). CSIRO-ARCCSS ACCESS-CM2 model output prepared for CMIP6 ScenarioMIP ssp585. Earth System Grid Federation. doi:https://doi.org/10.22033/ESGF/CMIP6.4332 .
CSIRO	**ACCESS-ESM1-5**	Ziehn et al. (2019). CSIRO ACCESS-ESM1.5 model output prepared for CMIP6 CMIP historical. Earth System Grid Federation. doi:https://doi.org/10.22033/ESGF/CMIP6.4272 .	Ziehn et al. (2019). CSIRO ACCESS-ESM1.5 model output prepared for CMIP6 ScenarioMIP ssp126. Earth System Grid Federation. doi:https://doi.org/10.22033/ESGF/CMIP6.4320 .			Ziehn et al. (2019). CSIRO ACCESS-ESM1.5 model output prepared for CMIP6 ScenarioMIP ssp585. Earth System Grid Federation. doi:https://doi.org/10.22033/ESGF/CMIP6.4333 .
AWI	**AWI-CM-1-1-MR**	Semmler et al. (2018). AWI AWI-CM1.1MR model output prepared for CMIP6 CMIP historical. Earth System Grid Federation. doi:https://doi.org/10.22033/ESGF/CMIP6.2686 .	Semmler et al. (2018). AWI AWI-CM1.1MR model output prepared for CMIP6 ScenarioMIP ssp126. Earth System Grid Federation. doi:https://doi.org/10.22033/ESGF/CMIP6.2796 .	Semmler et al. (2018). AWI AWI-CM1.1MR model output prepared for CMIP6 ScenarioMIP ssp245. Earth System Grid Federation. doi:https://doi.org/10.22033/ESGF/CMIP6.2800 .	Semmler et al. (2019). AWI AWI-CM1.1MR model output prepared for CMIP6 ScenarioMIP ssp370. Earth System Grid Federation. doi:https://doi.org/10.22033/ESGF/CMIP6.2803 .	Semmler et al. (2019). AWI AWI-CM1.1MR model output prepared for CMIP6 ScenarioMIP ssp585. Earth System Grid Federation. doi:https://doi.org/10.22033/ESGF/CMIP6.2817 .
BCC	**BCC-CSM2-MR**	Wu et al. (2018). BCC BCC-CSM2MR model output prepared for CMIP6 CMIP historical. Earth System Grid Federation. doi:https://doi.org/10.22033/ESGF/CMIP6.2948 .	Xin et al. (2019). BCC BCC-CSM2MR model output prepared for CMIP6 ScenarioMIP ssp126. Earth System Grid Federation. doi:https://doi.org/10.22033/ESGF/CMIP6.3028 .	Xin et al. (2019). BCC BCC-CSM2MR model output prepared for CMIP6 ScenarioMIP ssp245. Earth System Grid Federation. doi:https://doi.org/10.22033/ESGF/CMIP6.3030 .	Xin et al. (2019). BCC BCC-CSM2MR model output prepared for CMIP6 ScenarioMIP ssp370. Earth System Grid Federation. doi:https://doi.org/10.22033/ESGF/CMIP6.3035 .	Xin et al. (2019). BCC BCC-CSM2MR model output prepared for CMIP6 ScenarioMIP ssp585. Earth System Grid Federation. doi:https://doi.org/10.22033/ESGF/CMIP6.3050 .
CAS	**CAS-ESM2-0**	Chai, Zhaoyang (2020). CAS CAS-ESM1.0 model output prepared for CMIP6 CMIP historical. Earth System Grid Federation. doi:https://doi.org/10.22033/ESGF/CMIP6.3353 .	(2018). CAS CAS-ESM1.0 model output prepared for CMIP6 ScenarioMIP ssp126. Earth System Grid Federation. http://cera-www.dkrz.de/WDCC/meta/CMIP6/CMIP6.ScenarioMIP.CAS.CAS-ESM2-0.ssp126	(2018). CAS CAS-ESM1.0 model output prepared for CMIP6 ScenarioMIP ssp245. Earth System Grid Federation. http://cera-www.dkrz.de/WDCC/meta/CMIP6/CMIP6.ScenarioMIP.CAS.CAS-ESM2-0.ssp245	(2018). CAS CAS-ESM1.0 model output prepared for CMIP6 ScenarioMIP ssp370. Earth System Grid Federation. http://cera-www.dkrz.de/WDCC/meta/CMIP6/CMIP6.ScenarioMIP.CAS.CAS-ESM2-0.ssp370	(2018). CAS CAS-ESM1.0 model output prepared for CMIP6 ScenarioMIP ssp585. Earth System Grid Federation. http://cera-www.dkrz.de/WDCC/meta/CMIP6/CMIP6.ScenarioMIP.CAS.CAS-ESM2-0.ssp585
NCAR	**CESM2-WACCM**	Danabasoglu, Gokhan (2019). NCAR CESM2-WACCM model output prepared for CMIP6 CMIP historical. Earth System Grid Federation. doi:https://doi.org/10.22033/ESGF/CMIP6.10071 .	Danabasoglu, Gokhan (2019). NCAR CESM2-WACCM model output prepared for CMIP6 ScenarioMIP ssp126. Earth System Grid Federation. doi:https://doi.org/10.22033/ESGF/CMIP6.10100 .	Danabasoglu, Gokhan (2019). NCAR CESM2-WACCM model output prepared for CMIP6 ScenarioMIP ssp245. Earth System Grid Federation. doi:https://doi.org/10.22033/ESGF/CMIP6.10101 .	Danabasoglu, Gokhan (2019). NCAR CESM2-WACCM model output prepared for CMIP6 ScenarioMIP ssp370. Earth System Grid Federation. doi:https://doi.org/10.22033/ESGF/CMIP6.10102 .	Danabasoglu, Gokhan (2019). NCAR CESM2-WACCM model output prepared for CMIP6 ScenarioMIP ssp585. Earth System Grid Federation. doi:https://doi.org/10.22033/ESGF/CMIP6.10115 .

CMCC	**CMCC-CM2-SR5**	Lovato et al. (2020). CMCC CMCC-CM2-SR5 model output prepared for CMIP6 CMIP historical. Earth System Grid Federation. doi:https://doi.org/10.22033/ESGF/CMIP6.3825 .	Lovato et al. (2020). CMCC CMCC-CM2-SR5 model output prepared for CMIP6 ScenarioMIP ssp126. Earth System Grid Federation. doi:https://doi.org/10.22033/ESGF/CMIP6.3887 .	Lovato et al. (2020). CMCC CMCC-CM2-SR5 model output prepared for CMIP6 ScenarioMIP ssp245. Earth System Grid Federation. doi:https://doi.org/10.22033/ESGF/CMIP6.3889 .	Lovato et al. (2020). CMCC CMCC-CM2-SR5 model output prepared for CMIP6 ScenarioMIP ssp370. Earth System Grid Federation. doi:https://doi.org/10.22033/ESGF/CMIP6.3890 .	Lovato et al. (2020). CMCC CMCC-CM2-SR5 model output prepared for CMIP6 ScenarioMIP ssp585. Earth System Grid Federation. doi:https://doi.org/10.22033/ESGF/CMIP6.3896 .
CMCC	**CMCC-ESM2**	Lovato et al. (2021). CMCC CMCC-ESM2 model output prepared for CMIP6 CMIP historical. Earth System Grid Federation. doi:https://doi.org/10.22033/ESGF/CMIP6.13195 .	Lovato et al. (2021). CMCC CMCC-ESM2 model output prepared for CMIP6 ScenarioMIP ssp126. Earth System Grid Federation. doi:https://doi.org/10.22033/ESGF/CMIP6.13250 .	Lovato et al. (2021). CMCC CMCC-ESM2 model output prepared for CMIP6 ScenarioMIP ssp245. Earth System Grid Federation. doi:https://doi.org/10.22033/ESGF/CMIP6.13252 .	Lovato et al. (2021). CMCC CMCC-ESM2 model output prepared for CMIP6 ScenarioMIP ssp370. Earth System Grid Federation. doi:https://doi.org/10.22033/ESGF/CMIP6.13253 .	Lovato et al. (2021). CMCC CMCC-ESM2 model output prepared for CMIP6 ScenarioMIP ssp585. Earth System Grid Federation. doi:https://doi.org/10.22033/ESGF/CMIP6.13259 .
CCCMA	**CanESM5**	Swart et al. (2019). CCCma CanESM5 model output prepared for CMIP6 CMIP historical. Earth System Grid Federation. doi:https://doi.org/10.22033/ESGF/CMIP6.3610 .	Swart et al. (2019). CCCma CanESM5 model output prepared for CMIP6 ScenarioMIP ssp126. Earth System Grid Federation. doi:https://doi.org/10.22033/ESGF/CMIP6.3683 .	Swart et al. (2019). CCCma CanESM5 model output prepared for CMIP6 ScenarioMIP ssp245. Earth System Grid Federation. doi:https://doi.org/10.22033/ESGF/CMIP6.3685 .	Swart et al. (2019). CCCma CanESM5 model output prepared for CMIP6 ScenarioMIP ssp370. Earth System Grid Federation. doi:https://doi.org/10.22033/ESGF/CMIP6.3690 .	Swart et al. (2019). CCCma CanESM5 model output prepared for CMIP6 ScenarioMIP ssp585. Earth System Grid Federation. doi:https://doi.org/10.22033/ESGF/CMIP6.3696 .
E3SM-PROJECT	**E3SM-1-1**	Bader et al. (2019). E3SM-Project E3SM1.1 model output prepared for CMIP6 CMIP historical. Earth System Grid Federation. doi:https://doi.org/10.22033/ESGF/CMIP6.11485 .				Bader et al. (2020). E3SM-Project E3SM1.1 model output prepared for CMIP6 ScenarioMIP ssp585. Earth System Grid Federation. doi:https://doi.org/10.22033/ESGF/CMIP6.15179 .
EC-EARTH-CONSORTIUM	**EC-Earth3**	EC-Earth Consortium (EC-Earth) (2019). EC-Earth-Consortium EC-Earth3 model output prepared for CMIP6 CMIP historical. Earth System Grid Federation. doi:https://doi.org/10.22033/ESGF/CMIP6.4700 .	EC-Earth Consortium (EC-Earth) (2019). EC-Earth-Consortium EC-Earth3 model output prepared for CMIP6 ScenarioMIP ssp126. Earth System Grid Federation. doi:https://doi.org/10.22033/ESGF/CMIP6.4874 .	EC-Earth Consortium (EC-Earth) (2019). EC-Earth-Consortium EC-Earth3 model output prepared for CMIP6 ScenarioMIP ssp245. Earth System Grid Federation. doi:https://doi.org/10.22033/ESGF/CMIP6.4880 .	EC-Earth Consortium (EC-Earth) (2019). EC-Earth-Consortium EC-Earth3 model output prepared for CMIP6 ScenarioMIP ssp370. Earth System Grid Federation. doi:https://doi.org/10.22033/ESGF/CMIP6.4884 .	EC-Earth Consortium (EC-Earth) (2019). EC-Earth-Consortium EC-Earth3 model output prepared for CMIP6 ScenarioMIP ssp585. Earth System Grid Federation. doi:https://doi.org/10.22033/ESGF/CMIP6.4912 .
EC-EARTH-CONSORTIUM	**EC-Earth3-AerChem**	EC-Earth Consortium (EC-Earth) (2020). EC-Earth-Consortium EC-Earth3-AerChem model output prepared for CMIP6 CMIP historical. Earth System Grid Federation. doi:https://doi.org/10.22033/ESGF/CMIP6.4701 .			EC-Earth Consortium (EC-Earth) (2020). EC-Earth-Consortium EC-Earth3-AerChem model output prepared for CMIP6 ScenarioMIP ssp370. Earth System Grid Federation. doi:https://doi.org/10.22033/ESGF/CMIP6.4885 .	

EC-EARTH-CONSORTIUM	**EC-Earth3-CC**	EC-Earth Consortium (EC-Earth) (2021). EC-Earth-Consortium EC-Earth-3-CC model output prepared for CMIP6 CMIP historical. Earth System Grid Federation. doi:https://doi.org/10.22033/ESGF/CMIP6.4702 .		EC-Earth Consortium (EC-Earth) (2021). EC-Earth-Consortium EC-Earth3-CC model output prepared for CMIP6 ScenarioMIP ssp245. Earth System Grid Federation. doi:https://doi.org/10.22033/ESGF/CMIP6.15631 .		EC-Earth Consortium (EC-Earth) (2021). EC-Earth-Consortium EC-Earth3-CC model output prepared for CMIP6 ScenarioMIP ssp585. Earth System Grid Federation. doi:https://doi.org/10.22033/ESGF/CMIP6.15636 .
EC-EARTH-CONSORTIUM	**EC-Earth3-Veg-LR**	EC-Earth Consortium (EC-Earth) (2020). EC-Earth-Consortium EC-Earth3-Veg-LR model output prepared for CMIP6 CMIP historical. Earth System Grid Federation. doi:https://doi.org/10.22033/ESGF/CMIP6.4707 .	EC-Earth Consortium (EC-Earth) (2020). EC-Earth-Consortium EC-Earth3-Veg-LR model output prepared for CMIP6 ScenarioMIP ssp126. Earth System Grid Federation. doi:https://doi.org/10.22033/ESGF/CMIP6.4877 .	EC-Earth Consortium (EC-Earth) (2020). EC-Earth-Consortium EC-Earth3-Veg-LR model output prepared for CMIP6 ScenarioMIP ssp245. Earth System Grid Federation. doi:https://doi.org/10.22033/ESGF/CMIP6.4883 .	EC-Earth Consortium (EC-Earth) (2020). EC-Earth-Consortium EC-Earth3-Veg-LR model output prepared for CMIP6 ScenarioMIP ssp370. Earth System Grid Federation. doi:https://doi.org/10.22033/ESGF/CMIP6.4887 .	EC-Earth Consortium (EC-Earth) (2020). EC-Earth-Consortium EC-Earth3-Veg-LR model output prepared for CMIP6 ScenarioMIP ssp585. Earth System Grid Federation. doi:https://doi.org/10.22033/ESGF/CMIP6.4915 .
CAS	**FGOALS-f3-L**	YU, Yongqiang (2019). CAS FGOALS-f3-L model output prepared for CMIP6 CMIP historical. Earth System Grid Federation. doi:https://doi.org/10.22033/ESGF/CMIP6.3355 .	YU, Yongqiang (2019). CAS FGOALS-f3-L model output prepared for CMIP6 ScenarioMIP ssp126. Earth System Grid Federation. doi:https://doi.org/10.22033/ESGF/CMIP6.3464 .	YU, Yongqiang (2019). CAS FGOALS-f3-L model output prepared for CMIP6 ScenarioMIP ssp245. Earth System Grid Federation. doi:https://doi.org/10.22033/ESGF/CMIP6.3468 .	YU, Yongqiang (2019). CAS FGOALS-f3-L model output prepared for CMIP6 ScenarioMIP ssp370. Earth System Grid Federation. doi:https://doi.org/10.22033/ESGF/CMIP6.3479 .	YU, Yongqiang (2019). CAS FGOALS-f3-L model output prepared for CMIP6 ScenarioMIP ssp585. Earth System Grid Federation. doi:https://doi.org/10.22033/ESGF/CMIP6.3502 .
CAS	**FGOALS-g3**	Li, Lijuan (2019). CAS FGOALS-g3 model output prepared for CMIP6 CMIP historical. Earth System Grid Federation. doi:https://doi.org/10.22033/ESGF/CMIP6.3356 .	Li, Lijuan (2019). CAS FGOALS-g3 model output prepared for CMIP6 ScenarioMIP ssp126. Earth System Grid Federation. doi:https://doi.org/10.22033/ESGF/CMIP6.3465 .	Li, Lijuan (2019). CAS FGOALS-g3 model output prepared for CMIP6 ScenarioMIP ssp245. Earth System Grid Federation. doi:https://doi.org/10.22033/ESGF/CMIP6.3469 .	Li, Lijuan (2019). CAS FGOALS-g3 model output prepared for CMIP6 ScenarioMIP ssp370. Earth System Grid Federation. doi:https://doi.org/10.22033/ESGF/CMIP6.3480 .	Li, Lijuan (2019). CAS FGOALS-g3 model output prepared for CMIP6 ScenarioMIP ssp585. Earth System Grid Federation. doi:https://doi.org/10.22033/ESGF/CMIP6.3503 .
FIO-QLNM	**FIO-ESM-2-0**	Song, Zhenya; Qiao, Fangli; Bao, Ying; Shu, Qi; Song, Yajuan; Yang, Xiaodan (2019). FIO-QLNM FIO-ESM2.0 model output prepared for CMIP6 CMIP historical. Earth System Grid Federation. doi:https://doi.org/10.22033/ESGF/CMIP6.9199 .	Song, Zhenya; Qiao, Fangli; Bao, Ying; Shu, Qi; Song, Yajuan; Yang, Xiaodan (2019). FIO-QLNM FIO-ESM2.0 model output prepared for CMIP6 ScenarioMIP ssp126. Earth System Grid Federation. doi:https://doi.org/10.22033/ESGF/CMIP6.9208 .	Song, Zhenya; Qiao, Fangli; Bao, Ying; Shu, Qi; Song, Yajuan; Yang, Xiaodan (2019). FIO-QLNM FIO-ESM2.0 model output prepared for CMIP6 ScenarioMIP ssp245. Earth System Grid Federation. doi:https://doi.org/10.22033/ESGF/CMIP6.9209 .		Song, Zhenya; Qiao, Fangli; Bao, Ying; Shu, Qi; Song, Yajuan; Yang, Xiaodan (2019). FIO-QLNM FIO-ESM2.0 model output prepared for CMIP6 ScenarioMIP ssp585. Earth System Grid Federation. doi:https://doi.org/10.22033/ESGF/CMIP6.9214 .
NOAA-GFDL	**GFDL-CM4**	Guo et al. (2018). NOAA-GFDL GFDL-CM4 model output historical. Earth System Grid Federation. doi:https://doi.org/10.22033/ESGF/CMIP6.8594 .		Guo et al. (2018). NOAA-GFDL GFDL-CM4 model output prepared for CMIP6 ScenarioMIP ssp245. Earth System Grid Federation. doi:https://doi.org/10.22033/ESGF/CMIP6.9263 .		Guo et al. (2018). NOAA-GFDL GFDL-CM4 model output prepared for CMIP6 ScenarioMIP ssp585. Earth System Grid Federation. doi:https://doi.org/10.22033/ESGF/CMIP6.9268 .

NOAA-GFDL	**GFDL-ESM4**	Krasting et al. (2018). NOAA-GFDL GFDL-ESM4 model output prepared for CMIP6 CMIP historical. Earth System Grid Federation. doi:https://doi.org/10.22033/ESGF/CMIP6.8597 .	John et al. (2018). NOAA-GFDL GFDL-ESM4 model output prepared for CMIP6 ScenarioMIP ssp126. Earth System Grid Federation. doi:https://doi.org/10.22033/ESGF/CMIP6.8684 .	John et al. (2018). NOAA-GFDL GFDL-ESM4 model output prepared for CMIP6 ScenarioMIP ssp245. Earth System Grid Federation. doi:https://doi.org/10.22033/ESGF/CMIP6.8686 .	John et al. (2018). NOAA-GFDL GFDL-ESM4 model output prepared for CMIP6 ScenarioMIP ssp370. Earth System Grid Federation. doi:https://doi.org/10.22033/ESGF/CMIP6.8691 .	John et al. (2018). NOAA-GFDL GFDL-ESM4 model output prepared for CMIP6 ScenarioMIP ssp585. Earth System Grid Federation. doi:https://doi.org/10.22033/ESGF/CMIP6.8706 .
CCCR-IITM	**IITM-ESM**	Choudhury et al. (2019). CCCR-IITM IITM-ESM model output prepared for CMIP6 CMIP historical. Earth System Grid Federation. doi:https://doi.org/10.22033/ESGF/CMIP6.3708 .		Singh et al. (2020). CCCR-IITM IITM-ESM model output prepared for CMIP6 ScenarioMIP ssp245. Earth System Grid Federation. doi:https://doi.org/10.22033/ESGF/CMIP6.14748 .	Gopinathan et al. (2020). CCCR-IITM IITM-ESM model output prepared for CMIP6 ScenarioMIP ssp370. Earth System Grid Federation. doi:https://doi.org/10.22033/ESGF/CMIP6.14749 .	Panickal et al. (2020). CCCR-IITM IITM-ESM model output prepared for CMIP6 ScenarioMIP ssp585. Earth System Grid Federation. doi:https://doi.org/10.22033/ESGF/CMIP6.14753 .
INM	**INM-CM4-8**	Volodin et al. (2019). INM INM-CM4-8 model output prepared for CMIP6 CMIP historical. Earth System Grid Federation. doi:https://doi.org/10.22033/ESGF/CMIP6.5069 .	Volodin et al. (2019). INM INM-CM4-8 model output prepared for CMIP6 ScenarioMIP ssp126. Earth System Grid Federation. doi:https://doi.org/10.22033/ESGF/CMIP6.12325 .	Volodin et al. (2019). INM INM-CM4-8 model output prepared for CMIP6 ScenarioMIP ssp245. Earth System Grid Federation. doi:https://doi.org/10.22033/ESGF/CMIP6.12327 .	Volodin et al. (2019). INM INM-CM4-8 model output prepared for CMIP6 ScenarioMIP ssp370. Earth System Grid Federation. doi:https://doi.org/10.22033/ESGF/CMIP6.12329 .	Volodin et al. (2019). INM INM-CM4-8 model output prepared for CMIP6 ScenarioMIP ssp585. Earth System Grid Federation. doi:https://doi.org/10.22033/ESGF/CMIP6.12337 .
INM	**INM-CM5-0**	Volodin et al. (2019). INM INM-CM5-0 model output prepared for CMIP6 CMIP historical. Earth System Grid Federation. doi:https://doi.org/10.22033/ESGF/CMIP6.5070 .	Volodin et al. (2019). INM INM-CM5-0 model output prepared for CMIP6 ScenarioMIP ssp126. Earth System Grid Federation. doi:https://doi.org/10.22033/ESGF/CMIP6.12326 .	Volodin et al. (2019). INM INM-CM5-0 model output prepared for CMIP6 ScenarioMIP ssp245. Earth System Grid Federation. doi:https://doi.org/10.22033/ESGF/CMIP6.12328 .	Volodin et al. (2019). INM INM-CM5-0 model output prepared for CMIP6 ScenarioMIP ssp370. Earth System Grid Federation. doi:https://doi.org/10.22033/ESGF/CMIP6.12330 .	Volodin et al. (2019). INM INM-CM5-0 model output prepared for CMIP6 ScenarioMIP ssp585. Earth System Grid Federation. doi:https://doi.org/10.22033/ESGF/CMIP6.12338 .
IPSL	**IPSL-CM5A2-INCA**	Bouche et al. (2020). IPSL IPSL-CM5A2-INCA model output prepared for CMIP6 CMIP historical. Earth System Grid Federation. doi:https://doi.org/10.22033/ESGF/CMIP6.13661 .			Boucher et al. (2020). IPSL IPSL-CM5A2-INCA model output prepared for CMIP6 ScenarioMIP ssp370. Earth System Grid Federation. doi:https://doi.org/10.22033/ESGF/CMIP6.15714 .	
IPSL	**IPSL-CM6A-LR**	Boucher et al. (2018). IPSL IPSL-CM6A-LR model output prepared for CMIP6 CMIP historical. Earth System Grid Federation. doi:https://doi.org/10.22033/ESGF/CMIP6.5195 .	Boucher et al. (2019). IPSL IPSL-CM6A-LR model output prepared for CMIP6 ScenarioMIP ssp126. Earth System Grid Federation. doi:https://doi.org/10.22033/ESGF/CMIP6.5262 .	Boucher et al. (2019). IPSL IPSL-CM6A-LR model output prepared for CMIP6 ScenarioMIP ssp245. Earth System Grid Federation. doi:https://doi.org/10.22033/ESGF/CMIP6.5264 .	Boucher et al. (2019). IPSL IPSL-CM6A-LR model output prepared for CMIP6 ScenarioMIP ssp370. Earth System Grid Federation. doi:https://doi.org/10.22033/ESGF/CMIP6.5265 .	Bouche et al. (2019). IPSL IPSL-CM6A-LR model output prepared for CMIP6 ScenarioMIP ssp585. Earth System Grid Federation. doi:https://doi.org/10.22033/ESGF/CMIP6.5271 .
NIMS-KMA	**KACE-1-0-G**	Byun et al. (2019). NIMS-KMA KACE1.0-G model output prepared for CMIP6 CMIP historical. Earth System Grid Federation. doi:https://doi.org/10.22033/ESGF/CMIP6.8378 .	Byun et al. (2019). NIMS-KMA KACE1.0-G model output prepared for CMIP6 ScenarioMIP ssp126. Earth System Grid Federation. doi:https://doi.org/10.22033/ESGF/CMIP6.8432 .	Byun et al. (2019). NIMS-KMA KACE1.0-G model output prepared for CMIP6 ScenarioMIP ssp245. Earth System Grid Federation. doi:https://doi.org/10.22033/ESGF/CMIP6.8435 .	Byun et al. (2019). NIMS-KMA KACE1.0-G model output prepared for CMIP6 ScenarioMIP ssp370. Earth System Grid Federation. doi:https://doi.org/10.22033/ESGF/CMIP6.8437 .	Byun et al. (2019). NIMS-KMA KACE1.0-G model output prepared for CMIP6 ScenarioMIP ssp585. Earth System Grid Federation. doi:https://doi.org/10.22033/ESGF/CMIP6.8456 .

MIROC	**MIROC6**	Tatebe et al. (2018). MIROC MIROC6 model output prepared for CMIP6 CMIP historical. Earth System Grid Federation. doi:https://doi.org/10.22033/ESGF/CMIP6.5603 .	Shiogama et al. (2019). MIROC MIROC6 model output prepared for CMIP6 ScenarioMIP ssp126. Earth System Grid Federation. doi:https://doi.org/10.22033/ESGF/CMIP6.5743 .	Shiogama et al. (2019). MIROC MIROC6 model output prepared for CMIP6 ScenarioMIP ssp245. Earth System Grid Federation. doi:https://doi.org/10.22033/ESGF/CMIP6.5746 .	Shiogama et al. (2019). MIROC MIROC6 model output prepared for CMIP6 ScenarioMIP ssp370. Earth System Grid Federation. doi:https://doi.org/10.22033/ESGF/CMIP6.5752 .	Shiogama et al. (2019). MIROC MIROC6 model output prepared for CMIP6 ScenarioMIP ssp585. Earth System Grid Federation. doi:https://doi.org/10.22033/ESGF/CMIP6.5771 .
MPI-M/DKRZ	**MPI-ESM1-2-HR**	Jungclaus et al. (2019). MPI-M MPI-ESM1.2-HR model output prepared for CMIP6 CMIP historical. Earth System Grid Federation. doi:https://doi.org/10.22033/ESGF/CMIP6.6594 .	Schupfner et al. (2019). DKRZ MPI-ESM1.2-HR model output prepared for CMIP6 ScenarioMIP ssp126. Earth System Grid Federation. doi:https://doi.org/10.22033/ESGF/CMIP6.4397 .	Schupfner et al. (2019). DKRZ MPI-ESM1.2-HR model output prepared for CMIP6 ScenarioMIP ssp245. Earth System Grid Federation. doi:https://doi.org/10.22033/ESGF/CMIP6.4398 .	Schupfner et al. (2019). DKRZ MPI-ESM1.2-HR model output prepared for CMIP6 ScenarioMIP ssp370. Earth System Grid Federation. doi:https://doi.org/10.22033/ESGF/CMIP6.4399 .	Schupfner et al. (2019). DKRZ MPI-ESM1.2-HR model output prepared for CMIP6 ScenarioMIP ssp585. Earth System Grid Federation. doi:https://doi.org/10.22033/ESGF/CMIP6.4403 .
MPI-M	**MPI-ESM1-2-LR**	Wieners et al. (2019). MPI-M MPI-ESM1.2-LR model output prepared for CMIP6 CMIP historical. Earth System Grid Federation. doi:https://doi.org/10.22033/ESGF/CMIP6.6595 .	Wieners et al. (2019). MPI-M MPI-ESM1.2-LR model output prepared for CMIP6 ScenarioMIP ssp126. Earth System Grid Federation. doi:https://doi.org/10.22033/ESGF/CMIP6.6690 .	Wieners et al. (2019). MPI-M MPI-ESM1.2-LR model output prepared for CMIP6 ScenarioMIP ssp245. Earth System Grid Federation. doi:https://doi.org/10.22033/ESGF/CMIP6.6693 .	Wieners et al. (2019). MPI-M MPI-ESM1.2-LR model output prepared for CMIP6 ScenarioMIP ssp370. Earth System Grid Federation. doi:https://doi.org/10.22033/ESGF/CMIP6.6695 .	Wieners et al. (2019). MPI-M MPI-ESM1.2-LR model output prepared for CMIP6 ScenarioMIP ssp585. Earth System Grid Federation. doi:https://doi.org/10.22033/ESGF/CMIP6.6705 .
MRI	**MRI-ESM2-0**	Yukimoto et al. (2019). MRI MRI-ESM2.0 model output prepared for CMIP6 CMIP historical. Earth System Grid Federation. doi:https://doi.org/10.22033/ESGF/CMIP6.6842 .	Yukimoto et al. (2019). MRI MRI-ESM2.0 model output prepared for CMIP6 ScenarioMIP ssp126. Earth System Grid Federation. doi:https://doi.org/10.22033/ESGF/CMIP6.6909 .	Yukimoto et al. (2019). MRI MRI-ESM2.0 model output prepared for CMIP6 ScenarioMIP ssp245. Earth System Grid Federation. doi:https://doi.org/10.22033/ESGF/CMIP6.6910 .	Yukimoto et al. (2019). MRI MRI-ESM2.0 model output prepared for CMIP6 ScenarioMIP ssp370. Earth System Grid Federation. doi:https://doi.org/10.22033/ESGF/CMIP6.6915 .	Yukimoto et al. (2019). MRI MRI-ESM2.0 model output prepared for CMIP6 ScenarioMIP ssp585. Earth System Grid Federation. doi:https://doi.org/10.22033/ESGF/CMIP6.6929 .
NUIST	**NESM3**	Cao, Jian; Wang, Bin (2019). NUIST NESMv3 model output prepared for CMIP6 CMIP historical. Earth System Grid Federation. doi:https://doi.org/10.22033/ESGF/CMIP6.8769 .	Cao, Jian (2019). NUIST NESMv3 model output prepared for CMIP6 ScenarioMIP ssp126. Earth System Grid Federation. doi:https://doi.org/10.22033/ESGF/CMIP6.8780 .	Cao, Jian (2019). NUIST NESMv3 model output prepared for CMIP6 ScenarioMIP ssp245. Earth System Grid Federation. doi:https://doi.org/10.22033/ESGF/CMIP6.8781 .		Cao, Jian (2019). NUIST NESMv3 model output prepared for CMIP6 ScenarioMIP ssp585. Earth System Grid Federation. doi:https://doi.org/10.22033/ESGF/CMIP6.8790 .
NCC	**NorESM2-LM**	Seland et al. (2019). NCC NorESM2-LM model output prepared for CMIP6 CMIP historical. Earth System Grid Federation. doi:https://doi.org/10.22033/ESGF/CMIP6.8036 .	Seland et al. (2019). NCC NorESM2-LM model output prepared for CMIP6 ScenarioMIP ssp126. Earth System Grid Federation. doi:https://doi.org/10.22033/ESGF/CMIP6.8248 .	Seland et al. (2019). NCC NorESM2-LM model output prepared for CMIP6 ScenarioMIP ssp245. Earth System Grid Federation. doi:https://doi.org/10.22033/ESGF/CMIP6.8253 .	Seland et al. (2019). NCC NorESM2-LM model output prepared for CMIP6 ScenarioMIP ssp370. Earth System Grid Federation. doi:https://doi.org/10.22033/ESGF/CMIP6.8268 .	
NCC	**NorESM2-MM**	Bentsen et al. (2019). NCC NorESM2-MM model output prepared for CMIP6 CMIP historical. Earth System Grid Federation. doi:https://doi.org/10.22033/ESGF/CMIP6.8040 .	Bentsen et al. (2019). NCC NorESM2-MM model output prepared for CMIP6 ScenarioMIP ssp126. Earth System Grid Federation. doi:https://doi.org/10.22033/ESGF/CMIP6.8250 .	Bentsen et al. (2019). NCC NorESM2-MM model output prepared for CMIP6 ScenarioMIP ssp245. Earth System Grid Federation. doi:https://doi.org/10.22033/ESGF/CMIP6.8255 .	Bentsen et al. (2019). NCC NorESM2-MM model output prepared for CMIP6 ScenarioMIP ssp370. Earth System Grid Federation. doi:https://doi.org/10.22033/ESGF/CMIP6.8270 .	Bentsen et al. (2019). NCC NorESM2-MM model output prepared for CMIP6 ScenarioMIP ssp585. Earth System Grid Federation. doi:https://doi.org/10.22033/ESGF/CMIP6.8321 .

AS-RCEC	**TaiESM1**	Lee, Wei-Liang; Liang, Hsin-Chien (2020). AS-RCEC TaiESM1.0 model output prepared for CMIP6 CMIP historical. Earth System Grid Federation. doi:https://doi.org/10.22033/ESGF/CMIP6.9755 .	Lee, Wei-Liang; Liang, Hsin-Chien (2020). AS-RCEC TaiESM1.0 model output prepared for CMIP6 ScenarioMIP ssp126. Earth System Grid Federation. doi:https://doi.org/10.22033/ESGF/CMIP6.9806 .	Lee, Wei-Liang; Liang, Hsin-Chien (2020). AS-RCEC TaiESM1.0 model output prepared for CMIP6 ScenarioMIP ssp245. Earth System Grid Federation. doi:https://doi.org/10.22033/ESGF/CMIP6.9808 .	Lee, Wei-Liang; Liang, Hsin-Chien (2020). AS-RCEC TaiESM1.0 model output prepared for CMIP6 ScenarioMIP ssp370. Earth System Grid Federation. doi:https://doi.org/10.22033/ESGF/CMIP6.9809 .	Lee, Wei-Liang; Liang, Hsin-Chien (2020). AS-RCEC TaiESM1.0 model output prepared for CMIP6 ScenarioMIP ssp585. Earth System Grid Federation. doi:https://doi.org/10.22033/ESGF/CMIP6.9823 .

Supplementary Table 3 | Previous studies projecting forest-savanna transition (i.e., rainforest tipping) under future climate change.

Previous studies	Objective and methodology	Major assumptions	Main results
Parry et al. (2022)	– Objective: Evidence of Amazon rainforest dieback in CMIP6 models – Study area: Amazon – Model: Seven CMIP6-ESMs – Climate scenario: 1pctCO2 – Abrupt transitions/diebacks are detected based on vegetation carbon change of >2 kgC m^{-2} over 15 years. Furthermore, the change should be >25% of the initial vegetation carbon	– Dependent on ESM's projection of vegetation carbon estimates	– Exceeding 1.5°C will likely result in a sharp increase in the areas projected to experience diebacks (i.e., changes in vegetation carbon with temperature change). – Temperature seasonality trends are distinct for regions projected to experience dieback. – In most of the models, abrupt shifts are prominently observed for Guyana Shield (similar to our study)
Staal et al. (2020)	– Objective: Hysteresis of tropical forests under the 21st century climate – Study area: South America, Africa, and Australasia – Model: Seven CMIP6-ESMs; atmospheric moisture flows tracked using UTrack model – Climate scenario: SSP-8.5 – Hysteresis (both forest-to-savanna and savanna-to-forest) simulated by the end of the 21st century using the precipitation estimates from SSP5-8.5 (2071-2100). Stability landscape (i.e., based on alternative stable state theory) drawn using (empirical) precipitation (1970–1999) and tree cover (2000) data – Experiment: Hysteresis was simulated under two conditions: (i) a fully forested continent, and (ii) a fully deforested continent at the start of the simulation	– Stability landscape remains unchanged (defied for current climate) under the future climate change (i.e., pre-defined assumption on equilibrium states). This suggests that the influence of CO_2 fertilisation or nutrient limitation on stability landscape remains unaccounted – Moisture flows remain the same for future climate change. Influence of warming and land use change on altering moisture flow patterns (e.g., turbulence, wind patterns or ITCZ influence) is not accounted – Heterogeneous response of forests due to changes in soil characteristics or terrestrial species' intrinsic capacity to adapt not accounted	– Although Staal et al. (2020) look at hysteresis for (experiments) in a completely forested and deforested continent, the Guyana Shield doesn't recover back to forest regardless of the full forestation or deforestation scenario under future climate change. Thus, aligning with the results of this study – Similar to our study, the forest loss in Africa under future climate is not prominent as those observed under future climate change

Boulton et al. (2013)	– Objective: Early warning signals for detecting the tipping of the Amazon rainforests – Study area: Amazon – Model: HadCM3 Earth System model (ESM) – Climate scenario: Special Report on Emissions Scenarios (SRES) A1B scenario between 1860-2100 (historical spin-up prior to the year 2000) – Data on vegetation characteristics (specifically broadleaf fraction, vegetation carbon and net primary productivity) obtained from HadCM3	– Pre-defined thresholds for equilibrium states.	– Simulated forest dieback is not apparent from tree cover, vegetation carbon or net primary productivity. This could be both due to the model's own constraints in simulating tipping points, or; – due to the forceful simulation of vegetation equilibrium states in the climate models using rapid and non-linear forcings – This study suggests that the rise in variance could be an artefact of temperature and precipitation variability
Higgins and Scheiter (2012)	– Objective: Carbon assimilation in vegetation under changes in atmospheric CO_2 – Study area: Africa – Model: adaptive Dynamic Global Vegetation Model (aDGVM) – Climate scenario: CMIP3- SRES A1B. – aDGMV was used to simulate the shifts between forests, savannas and grasses between 1850 and 2100. – Experiment: Simulations were run at constant CO_2 concentrations of 170, 400 and 700 ppm; and ambient precipitation.	– Influence of land use change impacts and inter-annual variability in precipitation are ignored – Parametrisation of ecosystems phenological characteristics (e.g., carbon allocation to roots, shade tolerance) in the model	– Increase in tree dominance due to increase in atmospheric CO_2. However, uncertainty could arise due to them ignoring hydroclimate variability – This study acknowledges that the timing of such transitions depends on the stochastic fluctuations of other environmental factors, such as precipitation and fire
Jones et al. (2009)	– Objective: Terrestrial ecosystems' response to climate change – Study area: Exemplified for Amazon – Model: HadCM3LC, coupled with a dynamic vegetation TRIFFD – Climate scenario: CO_2 concentration (only) based on SRES A2 emissions scenario using Coupled Climate–Carbon Cycle Model Intercomparison Project (C4MIP) – State of the biosphere (i.e., the fraction of forest estimates) simulated by the model	– Dependent on TRIFFID's capability to simulate vegetation-climate feedbacks	– Loss of forest cover beyond 2°C rise in global warming – Even after climate stabilisation, the global terrestrial biosphere will continue to change due to the inertia of vegetation-climate feedbacks (i.e., vegetation-climate equilibrium). – Prominent loss of forests projected in the Guyana Shield part of the Amazon by 2050. These changes are not dynamic, but are referred to as 'committed' – signifying an accelerated equilibrium state if the climate forcings are left constant

Salazar et al. (2007)	– Aim: Influence of future climate change on biome distribution – Study area: South America – Model: Fifteen CMIP3-GCMs. – Climate scenarios: SRES (i) B1 – i.e., atmospheric CO_2 concentration reaches 550 ppm by 2100, and (ii) A2 – 860 ppm by 2100. – Experiment: The climatological estimates under these two scenarios were used to project future biome distribution using CPTEC-PVM vegetation model	– Biome distribution is dependent on climatological estimates and vegetation models' capacity to simulate vegetation-climate feedbacks	– Tropical forests will decrease by 18% by the end of the 21^{st} century (2090-2099) – Forest-to-savanna transition occurs in the south-eastern extent of the Amazonian rainforests
Cox et al. (2004)	– Aim: Amazon rainforests response to climate change – Study area: Amazon – Model: Global climate model HadCM3LC, coupled with a dynamic vegetation model TRIFFID – Climate scenario: CO_2 concentration (only) scenario based on IS92a 'business as usual'; and 980 ppmv by end of 21^{st} century	– Rate of soil respiration is assumed to double every 10K increase in temperature – Plant maintenance respiration increases with an increase in temperature – Dependent on the TRIFFID's capability to simulate vegetation-climate feedbacks (including all parametrisation related to CO_2 fertilisation and root zone dynamics). Influence of phosphorus limitation is ignored in the model	– High CO_2 concentration leads to suppression of rainfall across northern Amazonia, primarily due to changes in sea surface temperature – The CO_2-fertilisation-induced stomata closure and associated drying will lead to large-scale forest dieback, the impact of which will most prominently be observed in the second half of the 21^{st} century – The location of these risks is dependent on vegetation-climate feedbacks, and the individual model's capacity to simulate them

Supplementary References

de Boer-Euser, T., McMillan, H. K., Hrachowitz, M., Winsemius, H. C., and Savenije, H. H. G.: Influence of soil and climate on root zone storage capacity, Water Resources Research, 52, 2009–2024, https://doi.org/10.1002/2015WR018115, 2016.

Boulton, C. A., Good, P., and Lenton, T. M.: Early warning signals of simulated Amazon rainforest dieback, Theor Ecol, 6, 373–384, https://doi.org/10.1007/s12080-013-0191-7, 2013.

Boulton, C. A., Lenton, T. M., and Boers, N.: Pronounced loss of Amazon rainforest resilience since the early 2000s, Nat. Clim. Chang., 12, 271–278, https://doi.org/10.1038/s41558-022-01287-8, 2022.

Carpenter, S. R. and Brock, W. A.: Rising variance: a leading indicator of ecological transition, Ecology Letters, 9, 311–318, https://doi.org/10.1111/j.1461-0248.2005.00877.x, 2006.

skextremes Documentation: https://github.com/kikocorreoso/scikit-extremes.

Cox, P. M., Betts, R. A., Collins, M., Harris, P. P., Huntingford, C., and Jones, C. D.: Amazonian forest dieback under climate-carbon cycle projections for the 21st century, Theor Appl Climatol, 78, 137–156, https://doi.org/10.1007/s00704-004-0049-4, 2004.

Dakos, V., Scheffer, M., van Nes, E. H., Brovkin, V., Petoukhov, V., and Held, H.: Slowing down as an early warning signal for abrupt climate change, Proceedings of the National Academy of Sciences, 105, 14308–14312, https://doi.org/10.1073/pnas.0802430105, 2008.

GlobCover land-use map: http://due.esrin.esa.int/page_globcover.php, last access: 27 February 2022.

Gao, H., Hrachowitz, M., Schymanski, S. J., Fenicia, F., Sriwongsitanon, N., and Savenije, H. H. G.: Climate controls how ecosystems size the root zone storage capacity at catchment scale: Root zone storage capacity in catchments, Geophysical Research Letters, 41, 7916–7923, https://doi.org/10.1002/2014GL061668, 2014.

Gumbel, E. J.: Statistics of extremes., Columbia University Press, New York, 1958.

Higgins, S. I. and Scheiter, S.: Atmospheric CO2 forces abrupt vegetation shifts locally, but not globally, Nature, 488, 209–212, https://doi.org/10.1038/nature11238, 2012.

Hirota, M., Holmgren, M., Van Nes, E. H., and Scheffer, M.: Global Resilience of Tropical Forest and Savanna to Critical Transitions, Science, 334, 232–235, https://doi.org/10.1126/science.1210657, 2011.

Hurtt, G. C., Chini, L., Sahajpal, R., Frolking, S., Bodirsky, B. L., Calvin, K., Doelman, J. C., Fisk, J., Fujimori, S., Klein Goldewijk, K., Hasegawa, T., Havlik, P., Heinimann, A., Humpenöder, F., Jungclaus, J., Kaplan, J. O., Kennedy, J., Krisztin, T., Lawrence, D., Lawrence, P., Ma, L., Mertz, O., Pongratz, J., Popp, A., Poulter, B., Riahi, K., Shevliakova, E., Stehfest, E., Thornton, P., Tubiello, F. N., van Vuuren, D. P., and Zhang, X.: Harmonization of global land use change and management for the period 850–2100 (LUH2) for CMIP6, Geoscientific Model Development, 13, 5425–5464, https://doi.org/10.5194/gmd-13-5425-2020, 2020.

Jones, C., Lowe, J., Liddicoat, S., and Betts, R.: Committed terrestrial ecosystem changes due to climate change, Nature Geosci, 2, 484–487, https://doi.org/10.1038/ngeo555, 2009.

Parry, I. M., Ritchie, P. D. L., and Cox, P. M.: Evidence of localised Amazon rainforest dieback in CMIP6 models, Earth System Dynamics, 13, 1667–1675, https://doi.org/10.5194/esd-13-1667-2022, 2022.

Rocha, J. C.: Ecosystems are showing symptoms of resilience loss, Environ. Res. Lett., 17, 065013, https://doi.org/10.1088/1748-9326/ac73a8, 2022.

Salazar, L. F., Nobre, C. A., and Oyama, M. D.: Climate change consequences on the biome distribution in tropical South America, Geophysical Research Letters, 34, https://doi.org/10.1029/2007GL029695, 2007.

Scheffer, M., Bascompte, J., Brock, W. A., Brovkin, V., Carpenter, S. R., Dakos, V., Held, H., van Nes, E. H., Rietkerk, M., and Sugihara, G.: Early-warning signals for critical transitions, Nature, 461, 53–59, https://doi.org/10.1038/nature08227, 2009.

Singh, C., Wang-Erlandsson, L., Fetzer, I., Rockström, J., and van der Ent, R.: Rootzone storage capacity reveals drought coping strategies along rainforest-savanna transitions, Environ. Res. Lett., 15, 124021, https://doi.org/10.1088/1748-9326/abc377, 2020.

Singh, C., van der Ent, R., Wang-Erlandsson, L., and Fetzer, I.: Hydroclimatic adaptation critical to the resilience of tropical forests, Global Change Biology, 28, 2930–2939, https://doi.org/10.1111/gcb.16115, 2022.

Staal, A., Tuinenburg, O. A., Bosmans, J. H. C., Holmgren, M., van Nes, E. H., Scheffer, M., Zemp, D. C., and Dekker, S. C.: Forest-rainfall cascades buffer against drought across the Amazon, Nature Climate Change, 8, 539–543, https://doi.org/10.1038/s41558-018-0177-y, 2018.

Staal, A., Fetzer, I., Wang-Erlandsson, L., Bosmans, J. H. C., Dekker, S. C., van Nes, E. H., Rockström, J., and Tuinenburg, O. A.: Hysteresis of tropical forests in the 21st century, Nat Commun, 11, 4978, https://doi.org/10.1038/s41467-020-18728-7, 2020.

Walsh, R. P. D. and Lawler, D. M.: Rainfall Seasonality: Description, Spatial Patterns and Change Through Time, Weather, 36, 201–208, https://doi.org/10.1002/j.1477-8696.1981.tb05400.x, 1981.

Wang-Erlandsson, L., Bastiaanssen, W. G. M., Gao, H., Jägermeyr, J., Senay, G. B., van Dijk, A. I. J. M., Guerschman, J. P., Keys, P. W., Gordon, L. J., and Savenije, H. H. G.: Global root zone storage capacity from satellite-based evaporation, Hydrology and Earth System Sciences, 20, 1459–1481, https://doi.org/10.5194/hess-20-1459-2016, 2016.

Zemp, D. C., Schleussner, C.-F., Barbosa, H. M. J., Hirota, M., Montade, V., Sampaio, G., Staal, A., Wang-Erlandsson, L., and Rammig, A.: Self-amplified Amazon forest loss due to vegetation-atmosphere feedbacks, Nature Communications, 8, 14681, https://doi.org/10.1038/ncomms14681, 2017.